Using Physiography to Understand Stream Network Expansion and Contraction Across Spatiotemporal Scales

Delaney M. Peterson[1,2], C. Nathan Jones[1], Kaci Zarek[1,3], Michelle Wolford[1], Chelsea R. Smith[1], Charles T. Bond[4], Stephen Plont[1], Maggi Kraft[5], Shannon Speir[6], Sam Zipper[7,8], Sarah E. Godsey[5], Jonathan P. Benstead[1], Arial J. Shogren[1], Kevin A. Kuehn[4], and Carla L. Atkinson[1]

[1]Department of Biological Sciences, University of Alabama, Tuscaloosa, AL, USA.

[2]Department of Biological and Ecological Engineering, Oregon State University, Corvallis, OR, USA.

[3]Department of Ecology and Evolutionary Biology, Cornell University, Ithaca, NY, USA.

[4]School of Biological, Environmental, and Earth Sciences, University of Southern Mississippi, Hattiesburg, MS, USA.

[5]Department of Geosciences, Idaho State University, Pocatello, ID, USA.

[6]Department of Crop, Soil, and Environmental Sciences, University of Arkansas, Fayetteville, AR, USA.

[7]Kansas Geological Survey, University of Kansas, Lawrence, KS, USA.

[8]Department of Geology, University of Kansas, Lawrence, KS, USA.

Corresponding author: Delaney Peterson (dmpeterson2@crimson.ua.edu)

This is a non-peer-reviewed manuscript being submitted to Water Resources Research

Key Points:

- Low-relief watersheds do not conform to contemporary perceptual models of stream network expansion and contraction.
- A combination of topographic, geologic, and vegetative drivers best explained the stream network variability observed in our watersheds.
- Sensor placement matters: expanding sensors to hydrologically variable reaches increased the significance of topography in network dynamics.

Abstract

Non-perennial streams (i.e., streams that cease flowing regularly across time or space) comprise ~60% of the global river network and play an important role in the physical, chemical, and biological functions of downstream waters. However, predicting their patterns of network expansion and contraction remains a key challenge across regulatory, practitioner, and research communities, especially given that most investigations focus on high-relief watersheds. To address this challenge, we employed physiography as a lens to investigate the impacts of geology, soil characteristics, topography, and vegetation on spatial and temporal patterns of stream wetting and drying. We instrumented three headwater stream networks located in the Coastal Plain, Piedmont, and Appalachian Plateaus physiographic provinces in the southeastern United States. In each network, we used ≥ 20 water presence/absence sensors over two water years (2023 and 2024) to investigate seasonal and interannual variability in network extent. Across the physiographic gradient, we found that a combination of topographic, geologic, and vegetative drivers best explained variability in stream network persistence. Our results also emphasized the role that sensor placement plays in understanding network-scale patterns, as deploying sensors in areas of greatest hydrologic variability was crucial to capturing the full range of network expansion and contraction. This study demonstrated that low-relief stream networks challenge contemporary perceptual models of network dynamics, and that consideration of other factors such as soils and vegetation can help explain network expansion and contraction in low-relief headwater stream networks.

Plain Language Summary

Streams that stop flowing regularly across space or time make up large portions of river systems and play important roles in the quantity and quality of water reaching larger rivers. However, it is still difficult to predict where and how stream network length changes through time, as previous work has mainly focused on stream drying in mountainous watersheds. This makes it challenging to regulate, manage, and research stream networks effectively, particularly in less mountainous regions. To address this challenge, we investigated stream network length across time and space by considering the topography, geology, soil, and plant community structure of landscapes, or their physiography. We placed at least 20 sensors that measured water presence in each of three watersheds to understand changes in network length throughout seasons and between years. We

found that network length in our three gently sloping watersheds was influenced by variables from all components of physiography. We also found that the location of the sensors influenced patterns in observable stream length. Altogether, this study demonstrates the importance of considering systems with little elevation change, as well as drivers in addition to topography, to better predict how the length of stream networks changes through time.

1 Introduction

Streams are inherently dynamic features on the landscape (Godsey & Kirchner, 2014), as their response to inputs from precipitation and subsurface storage zones can manifest as significant streamflow variation at daily to decadal scales. Non-perennial streams are portions of the stream network that cease flowing regularly across either space or time (Busch et al., 2020), often in headwater segments of the network that expand and contract dynamically. Non-perennial streams constitute at least 60% of global river networks (Messager et al., 2021) and have important impacts on their downstream reaches (Brinkerhoff et al., 2024; Zimmer et al., 2022) by providing diverse and unique habitat (e.g., Datry et al., 2018), generating unique biogeochemical signals (e.g., Bernal et al., 2019; Gómez-Gener et al., 2021; Zarek et al., 2025), and contributing to seasonal flow and groundwater recharge (e.g., Zimmer & McGlynn, 2017). However, our understanding of the patterns of longitudinal network expansion and contraction and the processes they control has been biased towards quantifying patterns in streamflow variability related to the watershed outlet, rather than distributed patterns in network extent variability (but see Botter & Durighetto, 2020; Godsey & Kirchner, 2014; Prancevic et al., 2025; Prancevic & Kirchner, 2019). Therefore, identifying the primary drivers of variability in network length across systems is required to predict how non-perennial streams drive spatiotemporal variation in network connectivity.

Watershed physiographic characteristics exert strong control over hydrologic processes and network extent. Many studies have documented how meteorology, geology, and land cover act as first-order controls on streamflow and network expansion and contraction across river systems (e.g., Costigan et al., 2016; Hammond et al., 2021; Hynes, 1975; Zipper et al., 2021). Additionally, recent investigations on controls of network expansion and contraction have investigated the role of watershed topography, suggesting that flow convergence and valley transmissivity drive patterns in network expansion and contraction by regulating both the volume

of subsurface storage and rate of down-valley flow (Godsey & Kirchner, 2014; Prancevic & Kirchner, 2019). However, other studies have found that finer-scale watershed heterogeneity in soil properties (e.g., Gutiérrez-Jurado et al., 2019; Warix et al., 2023) or riparian vegetation (e.g., Newcomb & Godsey, 2023) can exert stronger controls on network extent dynamics than topography. Therefore, a clear picture of the hierarchical drivers on flowing network extent is lacking.

Our current understanding of network expansion and contraction is biased toward temporally low resolution measurements of high-relief systems. To date, a large proportion of hydrologic research has been conducted in montane, temperate, high-rainfall watersheds (Burt & McDonnell, 2015; McMillan et al., 2023). Studies of network expansion and contraction follow suit, with most studies being conducted in high-relief locations. For example, Botter et. al, (2024) and Ward et al., (2018) characterized stream network dynamics in the Swiss Alps and the Cascades in northwestern USA, respectively. Moreover, most of these studies use spatially high resolution network mapping techniques (e.g., Zimmer & McGlynn, 2018). While this stream-walking technique provides a spatially dense representation of the flowing channel, temporal resolution is typically limited to seasonal or monthly measurements. Recent advancements in low-cost sensors (e.g., Jensen et al., 2019) help bridge this gap by providing temporally dense point measures of water presence or absence across a network. However, sensor placement strategies are optimized for individual study objectives, making it difficult to synthesize these point observations into expansion and contraction dynamics across different networks. Moreover, many sensor-based studies have also been located in high-relief systems (e.g., Dohman et al., 2021; Kindred, 2022; Warix et al., 2023). This highlights the need to further develop uniform approaches to sensor deployment to better characterize the drivers of network dynamics across more diverse physiographic settings.

One potential framework for understanding the hierarchical drivers of network extent is physiography. Physiography is generally defined as the geologic, topographic, and biotic features of the landscape (Fenneman, 1938), thereby integrating multiple potential drivers of network expansion and contraction to provide a more holistic view of the watershed setting. Physiography has been one of the primary tools that has been operationalized by researchers and managers to classify the physical templates of landscapes, and its hierarchical nature lends itself well to studies at a variety of scales. In the US, Fenneman and others (1938) classified the entire country

into physiographic provinces, sections, and districts based on existing records of soils, geology, and resulting vegetative communities. In this mapping effort, physiographic provinces (e.g., Coastal Plain) are the coarsest resolution and were originally defined based on broad geomorphic characteristics to identify relatively similar regions across large spatial scales (Fenneman 1938). Subordinate sections (e.g., East Gulf Coastal Plain) and smaller districts (e.g., Fall Line Hills) were based on the same characteristics, but at increasingly higher resolutions to identify similar regions at more localized scales. Therefore, physiography provides a consistent and useful template for conducting hydrologic studies, as watersheds located in the same physiographic provinces should have comparable watershed characteristics.

To quantify the effects of physiography on network expansion and contraction, we focus on hydrologic connectivity, broadly defined as the water-mediated movement of materials, organisms, and energy (Pringle, 2001; Rinderer et al., 2018). Hydrologic connectivity incorporates flows across vertical, lateral, and longitudinal dimensions, as well as through time (Harvey & Gooseff, 2015; Ward, 1989; Zimmer & McGlynn, 2018). Hydrologic connectivity also provides a unifying framework for evaluating water fluxes across spatiotemporal scales as well as disciplines (Jones et al., 2019). Here, we focus on network connectivity in the longitudinal dimension at the watershed scale, and define this connectivity as network expansion, contraction, and fragmentation through time. While many studies have paired longitudinal connectivity with observations of discharge at the outlet to investigate the impacts of flow and network variability on biogeochemical fluxes (e.g., Zarek et al., 2025; Zimmer & McGlynn, 2018), fewer studies have focused on the dynamics of longitudinal connectivity as an integrator of within-watershed hydrologic processes.

In this study, our goal was to investigate the interactions between stream network expansion/contraction and watershed characteristics using physiography as a template to understand network extent dynamics. In the southeastern USA, a natural physiographic gradient forms as the Appalachian mountains grade into coastal regions. Further, this gradient is complemented by a generally uniform climate; much of the southeastern USA receives similar precipitation inputs regardless of physiographic region. Therefore, to test potential drivers of network connectivity, we instrumented three watersheds across this physiographic gradient as a natural experiment – one in the Coastal Plain, one in the Piedmont, and one in the Appalachian Plateaus. While these watersheds extend from the mountains to the coast, we stress that these

watersheds are all low-relief relative to other studies (they all exhibit less than 350 m of relief across areas of 3 km^2 or less). We deployed a standardized network of water presence/absence sensors in each watershed, and used these to monitor site- and network-scale flow dynamics across two water years of contrasting dryness (2023 and 2024). We used this sensor network to address our research objectives: (i) characterize the spatial and temporal patterns and drivers of network connectivity and surface water persistence across a relatively low-relief region, (ii) investigate the role physiographic variables (i.e., topography, underlying geology, and vegetation) play in watershed-scale network expansion and contraction, (iii) evaluate the role of sensor placement on network-scale metrics of connectivity.

2 Methods

2.1 Site Descriptions

We instrumented three watersheds across a physiographic gradient in Alabama (USA; Figure 1A). Each watershed was selected to represent the general watershed structure of its larger physiographic province, while also containing non-perennial, headwater portions of the larger stream network. Our watersheds were small and generally similar in size (~1 km^2), and we used a standardized site design to maximize comparability between networks (*see Section 2.2.1*). All three watersheds had a comparable climatic setting, allowing us to investigate watershed controls across regions without confounding climatic factors. These watersheds all had a humid subtropical climate, with a mean annual precipitation ranging from 1,350 to 1,400 mm per year, and mean annual air temperatures ranging from 15.3 to 17.8˚C (NOAA NCEI, 2025). This region receives generally consistent precipitation throughout the year with no obvious climatic dry season, though there is considerable intra- and interannual variability. However, high evapotranspiration (ET) rates in the late summer and early fall drive reductions in streamflow and a hydrologic dry season in this region (Czikowsky & Fitzjarrald, 2004; Hupp, 2000). We describe each research watershed below and outline their key components in Table 1. We recognize that there is considerable heterogeneity across headwater watersheds (Golden et al., 2025), and while some of the heterogeneity among our watersheds likely reflects broader regional differences, within-watershed observations probably do not capture the full range of conditions present throughout each region. Additional information about these watersheds can be

found in the Detailed Site Descriptions in *Text S1*, and information about additional concurrent data collection (e.g., precipitation, biogeochemistry, microbial ecology) can be found in Plont et al. (2025).

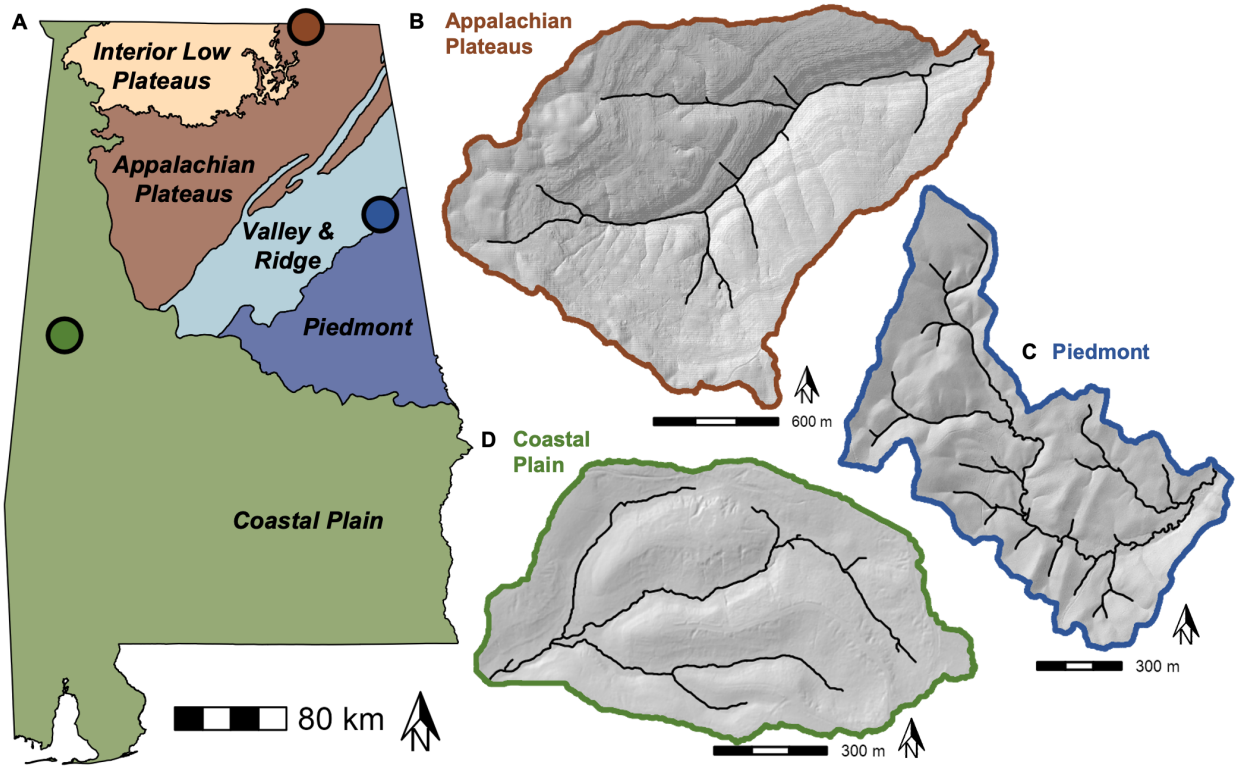

Figure 1. **(A)** A map of Alabama, USA colored by physiographic provinces. Each point corresponds to one of the three research watersheds, **(B-D)** which are also colored by physiographic province. **(B-D)** Hillshade maps of the three research watersheds, with the geomorphic channel network mapped by the black lines. Note: the point corresponding to the Piedmont research watershed obscures a portion of the boundary between the Valley and Ridge and Piedmont physiographic provinces; however, this watershed is entirely located in the Piedmont.

Table 1. *Watershed Characteristics*

Research watershed	Outlet location (Lat., Lon.)	Mean Jan. air temp. [˚C][a]	Mean Jul. air temp. [˚C][a]	Mean annual precip. (mm/yr)[a]	Elevation range (masl), (relief, m)	Water-shed area (km^2)	Watershed average (min., max.) slope (%)	Primary lithology	Primary soil texture[b]
Appalachian Plateaus	34.968617, -86.165017	4.4˚	25.4˚	1,390	211 - 550 (339)	2.97	17 % (0.01, 69)	Karstic sedimentary	Silty clay loam
Piedmont	33.762197, -85.595507	5.3˚	25.3˚	1,400	345 - 456 (111)	0.92	12 % (0.005, 49)	Low-grade fractured metamorphic	Silt loam
Coastal Plain	32.984109, -88.013343	7.3˚	27.4˚	1,350	63 - 94 (31)	0.70	7 % (0.001, 28)	Sedimentary marine deposits	Fine, sometimes sandy, loam

[a]Obtained from NOAA NCEI (2025).

[b]Obtained from Soil Survey Staff (2025).

2.1.1 Appalachian Plateaus research watershed

The watershed in the Appalachian Plateaus province drains a non-perennial tributary of Burks Creek in Jackson County, AL (USA; Figure 1B). There was 1,350 mm of precipitation in the 2023 water year and 1,300 mm in the 2024 water year (Table 1). While precipitation was below average during the study period, the previous water year (2022) had above-average precipitation of 1,540 mm. This watershed has the highest relief of our three study sites, and is underlain by karstic Mississippian-aged sedimentary lithologic units (Table 1). In the headwaters, there are abundant cave-springs at the exposure of the Bangor limestone unit, as well as spring discharges from numerous fractures (Ponta, 2018). The soils are very shallow in this watershed, primarily as a function of the steep stony slopes and geologic erosion (Swenson, 1954). The upper portions of the watershed have thin, organic soils primarily in the Mollisol soil order, and the streambeds are primarily exposed bedrock. Conversely, the soils in the lower portions of the watershed are highly weathered Ultisols, and stream sediment aggradation occurs in the lower portion of the network (Soil Survey Staff, 2025). This watershed is almost entirely forested with primarily deciduous species, and is privately owned and managed for hunting and conservation. This watershed, like much of the area, was used for silvicultural harvest until around the turn of the 20th century, resulting in a mixed-age forest (Swenson, 1954).

Additionally, portions of the valley bottom and several areas in the headwaters have been cleared for cultivation, but the majority of the riparian zone is forested.

2.1.2 Piedmont research watershed

The watershed in the Piedmont province drains a non-perennial tributary to Pendergrass Creek in Cleburne County, AL (USA, Figure 1C). There was 1,400 mm of precipitation in the 2023 water year and 1,390 mm in the 2024 water year (Table 1). This network drains a moderate-relief watershed, and is underlain by Silurian-Devonian-aged low-grade metamorphic lithologic units that have formed highly weathered soils (Table 1). The groundwater systems in this region are highly complex due to the fractured lithology, but the primary lithologic unit in this watershed is included in the metasedimentary and metavolcanic unconfined aquifer system (Kopaska-Merkel et al., 2000). This watershed is dominated by highly weathered Ultisols. The upper portions of the watershed have thin and rocky soils where the regolith is close to the surface (Feminella, 1996; Kopaska-Merkel et al., 2000), with primarily coarse stream sediments (i.e., gravel, pebbles, and cobbles). Conversely, the lower portion of the watershed has more developed, argillic soils, and the streambeds consist of a mix of coarse and fine-grained (i.e., sand, silt) sediments (Zarek et al., 2025). This watershed is entirely forested with mixed deciduous and coniferous species within the federally owned Talladega National Forest, and is managed for recreation, silviculture, and conservation.

2.1.3 Coastal Plain research watershed

The watershed in the Coastal Plain province drains a non-perennial tributary to Shambley Creek in Greene County, AL (USA; Figure 1D). There was 1,450 mm of precipitation in the 2023 water year and 1,250 mm in the 2024 water year (Table 1). This watershed has the lowest relief in our study, and is underlain by Upper Cretaceous-age sedimentary lithologic units that are composed primarily of sand and clay (Table 1). The watershed is dominated by highly weathered Ultisols, Alfisols with argillic horizons, and poorly organized Entisols (Soil Survey Staff, 2025). The stream substrate of this watershed is primarily fine-grained sediment (i.e., clay lenses, silt, sand), with some conglomerate pebbles near the watershed outlet. Further, the combination of highly erodible soils and low relief has resulted in highly incised portions of the network, with over half (55%) of the network incised > 0.5 m below the riparian zone, and some

areas of incision nearly 2 m deep. This watershed is entirely forested with mixed coniferous and deciduous species, and managed for rotational silvicultural harvest by the Weyerhaeuser Company. Within this watershed, the uplands are almost entirely pine species, with dense, primarily oak riparian vegetation. The southern upland portion of the watershed was thinned and harvested in the summer of 2024, but all vegetation within 11 m of the stream channel was preserved.

2.1.4 Within-watershed Hydrogeomorphic Features (HGFs)

We delineated each watershed into distinct units linked to their hydrologic functions known as hydrogeomorphic features (HGFs; following Peterson et al., 2025) to characterize the inherent variability of river corridor structure within our watersheds. Each HGF was assigned based on key structures across the river corridor that we identified in the field as potential regulators of hydrologic connectivity. Notably, these HGFs integrate topographic, geologic, and vegetative characteristics across the entire river corridor (i.e., the stream channel and adjacent riparian zones and hillslopes). In the Appalachian Plateaus, we delineated the network into two HGFs; HGF A1 was characterized by bedrock channels and steep slopes, and HGF A2 consisted of lower-gradient channels with sediment accumulation (*Figure S1*). In the Piedmont, we delineated the network into three similar units; HGF P1 had highly constrained valleys and steep slopes, HGF P2 consisted of wider valleys with coarse sediment, and HGF P3 was characterized by wide and densely vegetated riparian zones with low slopes (*Figure S2*). In the Coastal Plain, where the HGF framework was developed in Peterson et al. (2025), we delineated the network into three units; HGF C1 was defined as low-gradient reaches with high width-depth ratios, HGF C2 consisted of channels with distinct banks and evidence of over-bank flows, and HGF C3 had deeply entrenched (> 0.5 m of incision) channels that rarely inundated the adjacent riparian zone (*Figure S3*). By defining these HGFs as subunits of each watershed, we were then able to aggregate individual sites into similar groups to evaluate watershed characteristics that were only measurable at larger scales.

2.2 Hydrologic Monitoring Instrumentation

We instrumented each watershed with a network of water presence/absence sensors to quantify network length across time, as well as water persistence at each site. We also installed a

discharge monitoring station at the watershed outlet, and collected local meteorological data using weather stations located within 5 km of the watershed outlet. All sensors logged at concurrent 15-minute intervals from 1 Oct. 2022 through the spring of 2024, and then logged at concurrent hourly intervals from the spring of 2024 through Sep. 2024. While sensors were initially deployed in Sep. 2021, we only used data from the 2023 and 2024 water years in this study due to above-average precipitation in the 2022 water year that resulted in stable networks with minimal contraction.

2.2.1 Watershed-Scale Network Length Monitoring

Each watershed was instrumented with at least 20 Stream Temperature, Intermittency, and Conductivity (hereafter, STIC) sensors that measure water presence/absence (*sensu* Chapin et al., 2014; Jensen et al., 2019). We used a standardized site selection design based on the relationship between contributing area and topographic wetness index (TWI; outlined in Swenson et al., 2024; Zipper et al., 2025) to maximize comparability across networks. This resulted in sensor networks that spanned a gradient of TWI or potential wetness conditions, rather than a uniform density (Figure 2A-B). For an 11-month period (May 2022 through April 2023), we deployed an additional 29 STICs in the Piedmont watershed to capture a higher spatial resolution and extent of conditions across the watershed in coordination with a large synoptic sampling effort (June 2022; Plont et al., 2025). These additional STIC sensors were placed strategically to fill spatial gaps in the existing network, while also expanding up into the upstream ephemeral tips of the stream network. At each site, we placed STIC sensors in the thalweg at the highest point (i.e., the head of a riffle) within the reach selected by the standardized site design (Figure 2C). Sensors were anchored within 1 cm of the stream bed to capture low flows. We maintained and downloaded data from the sensors every 4-6 months and removed the sensors for 3-7 days to change the batteries every 9 months. During every maintenance visit, we also recorded water presence/absence at the site and height of the sensor relative to the streambed to validate sensor measurements.

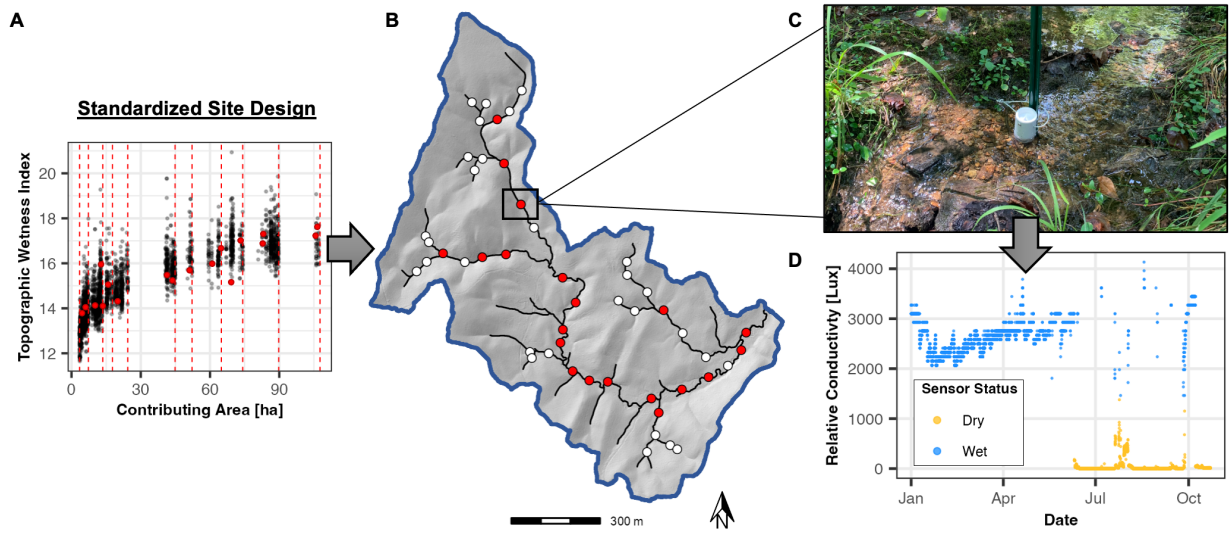

Figure 2. Standardized site design for sensor placement within each watershed network. **(A)** The distribution of cells within the watershed raster, binned by contributing area. Selected points are indicated in red. **(B)** The Piedmont watershed, with the selected site locations indicated in red. The additional 29 strategic locations are indicated in white. **(C)** An image of a STIC deployed in a stream reach. **(D)** An example output from the STIC, with relative conductivity (Lux; see Zipper et al., 2025 for details of data processing and units) across time, and the water presence/absence indicated by the color of each point. See *Figure S4* for sensor placement in the Appalachian Plateaus and Coastal Plain sites.

We used a project-specific data-processing pipeline to clean and quality-control STIC sensor data (Zipper et al., 2025). Briefly, for each individual sensor we identified thresholds of relative conductivity (measured in Lux as a legacy of the original sensor programming) for the transition from dry to wet by immersing each sensor in water with a specific conductivity of 0 µS/cm (i.e., the lowest possible relative conductivity reading corresponding to water presence; Burke et al., 2024) in the lab prior to deployment. We used these thresholds to convert the uncalibrated relative conductivity to a binary wet/dry metric (Godsey et al., 2024). For each sensor, we compared the resulting wet/dry record to field observations of water presence, and ensured that the defined thresholds yielded comparable results as well as manually adjusted the threshold to match field observations when necessary. We then quality-controlled all data by flagging any data that had negative conductivity readings or were identified as potential anomalies (i.e., a moving window z-score > 3), following Zipper et al. (2025). We removed any of these flagged observations that were obvious outliers following visual inspection, as well as

any periods where the sensor collected temperature, but not conductivity (Peterson & Jones 2025g; 2025h; 2025i). Finally, we filtered all data to periods of time where all sensors were recording concurrently to build our final dataset.

We then used the GPS locations of each sensor to calculate a representative reach length as the sum of half the distance from the downstream and upstream sensors, such that the reach was centered around the sensor of interest and accounted for tributaries. We used these sensor measurements to calculate the length of the active surface drainage network (hereafter, ASDN in m, *sensu* Zimmer & McGlynn, 2018) as the total length of the wet stream network. Here, we calculated ASDN length at sub-daily and daily timesteps by summing reach lengths for all wet sensors. Additionally, for each individual sensor, we calculated the local water persistence as the number of wet observations across the period of record divided by the total number of observations. Notably, streambed sediments in the southeastern USA are highly mobile, and streambed erosion and deposition imply that some of our sensor locations likely did not always remain the first to dry throughout the study as they were initially installed. Similarly, our assumption that each sensor represents its neighboring 100-500 m reach might not be accurate at every time point in this study. However, comparisons between these point observations and spatially continuous mapping show that sensors usually adequately represent network-scale dynamics (e.g., Kindred et al., 2022).

2.2.2 Watershed Outlet Discharge Monitoring

At the outlet of each watershed, we installed high-frequency monitoring stations that measured stream water level (meters) at the same 15-minute intervals, as well as a suite of other measurements (for more information, see Section 2.3 of Zarek et al., 2025 and Section 2.2.1 of Plont et al., 2025). The stream monitoring well was instrumented with a Seametrics PT12 pressure sensor that recorded relative stream water level from September 2021 until it was replaced by a stand-alone Onset HOBO U20L pressure transducer; this transition occurred in the Piedmont in January 2023, the Coastal Plain in June 2023, and the Appalachian Plateaus in June 2024. We converted the instantaneous water level measurements to absolute elevation (meters above sea level, hereafter masl) using channel geometry surveys and a co-located HOBO U20L pressure transducer to collect barometric pressure, and paired these data with rating curves

developed using salt dilution-gauging discharge measurements to develop a record of instantaneous discharge (in L/s) at 15-minute intervals at each watershed outlet for the study period (Plont, Speir et al., 2025a; 2025b; Plont, Wolford et al., 2025).

2.3 Physiographic Analyses

We calculated a suite of topographic, geospatial, and vegetative metrics to characterize the physiography of the three watersheds to contextualize our network results (*Table S1*). We calculated topographic, geologic, and pedologic metrics at both the site- and HGF-scales using publicly available data (e.g., DEMs from USGS, geology and soils data from NRCS) as well as geomorphometric tools from the *whitebox* package in R (Wu & Brown, 2022). Additionally, we used field data collected in tandem with this work to calculate vegetative metrics at the HGF scale. We paired these metrics with our network analyses (e.g., drainage density, curvature, and slope coefficients; Table 2) to identify the physiographic drivers of stream connectivity. All analyses were performed using R v4.4.0 (R Core Team, 2023).

2.3.1 Topographic Analysis

First, we obtained high-resolution (1-m or finer) DEMs for each of our watersheds from the USGS national map downloader v2.0 (https://apps.nationalmap.gov/downloader/). We processed these DEMs by filtering, filling pits, and breaching depressions using the respective *whitebox* functions in R (R Core Team, 2024; Wu & Brown, 2022). We then used the *wbt_watershed()* function to delineate our watersheds, and used the d8 flow direction and flow accumulation rasters to delineate our stream networks. In the field, we observed the maximum extent of the geomorphic channel network (characterized as vegetation-free areas of sediment deposition and accumulation). We then defined minimum flow accumulation thresholds for each watershed that yielded networks most closely matching the geomorphic channel network (60,000 1-m cells in the Appalachian Plateaus; 10,000 0.92-m cells in the Piedmont; 12,000 1-m cells in the Coastal Plain). These watersheds and stream networks were then used as the foundation for the rest of the topographic metrics.

We calculated site-specific topographic metrics at each sensor location to compare with our network metrics. We calculated elevation, slope at several scales (*Table S1*), drainage area,

distance to outlet, upstream network length, topographic wetness index (TWI), curvature, and aspect using the respective functions in the *whitebox* package (Wu & Brown, 2022), and topographic position index (TPI) by using the *multiscaleDTM* package (Ilich et al., 2025) to generate rasters of these variables. We then used the sensor location data snapped to the delineated stream network to extract the values of these variables for each location (Peterson & Jones 2025a; 2025b; 2025c). We calculated drainage density as a proxy for topographic convergence by dividing the upstream length by the drainage area for each location. Additionally, we calculated slope in a 5-m buffer zone (buffer slope, *Table S1*) around each sensor by averaging all cells in the buffer to integrate riparian and valley slope conditions near the sensor. We also calculated channel slope by generating a continuous stream slope raster and averaged the slope of all cells from the stream network raster in a 12.5-m buffer that equated to a 25-m stream reach.

We calculated the network-scale patterns in topographic variables following Prancevic & Kirchner (2019). Using the *elevatr* (Hollister, 2023) package, we extracted coarser 3-m DEMs to use in these analyses to reduce noise. We first calculated the drainage density for every point along the delineated channel networks, and extracted the exponent of the power-law relationship between drainage density and channel activation thresholds for the "ephemeral channel network" (α, defined as the portion of the network that we observed to have non-perennial flow; Prancevic & Kirchner, 2019). We then used the same slope raster described above to extract the exponent of the power-law relationship between slope and drainage area for the entire network (θ). Finally, we used *wbt_gaussian_filter()* within the *whitebox* package (Wu & Brown, 2022) to generate a 20-m smoothed DEM to calculate valley curvature. Using *wbt_mean_curvature()* in the *whitebox* package (Wu & Brown, 2022), we extracted curvature along the channel network, reversed the sign convention and doubled the output, following Prancevic & Kirchner (2019). We then calculated the exponent of the power-law relationship between curvature and drainage area (δ).

We also plotted stream network length as a function of outlet discharge to examine the relationship of stream network length to changes in flow, as well as the potential topographic controls on that relationship. This relationship has been related to the same three topographic drivers mentioned above: flow convergence, changes in gradient, and curvature. We first aggregated our temporally high resolution network length and discharge observations to daily

values by extracting only paired observations at 12 pm each day to reduce noise (*Table S3*). We then assessed the relationship of the stream network length as a function of discharge at the watershed outlet, and extracted the slope of the power-law relationship as our observed network expansion exponent (β; *Figure S6*). Additionally, we used the network-scale topographic patterns described above to calculate predicted β using Eqn. 4 in Prancevic & Kirchner (2019). Both the observed and predicted β allowed us to assess whether local topographic controls on network expansion and contraction aligned with global patterns observed in high-relief watersheds.

2.3.2 Geospatial Analysis

We gathered additional geologic and soils data at the HGF-scale using the NRCS Web Soil Survey. First, we used the Web Soil Survey to extract the primary soil map units within our watersheds (Soil Survey Staff, 2025). We then extracted depth to bedrock, saturated hydraulic conductivity, percentages of each soil texture class, organic matter content in the surficial 50 cm, and primary lithologic underlying units from each soil map unit (*Table S1*). We also used the soil maps within each watershed to extract these variables for each sensor location. We then aggregated these variables by HGF to evaluate relationships between these patterns at a more appropriate scale, as the Web Soil Survey was developed at a coarser resolution.

2.3.3 Vegetation Analysis

We derived relative proportions of vegetation types from densiometer measurements taken throughout the watershed across seasons. In short, densiometer measurements of canopy coverage were taken at seven consistent locations within each watershed at least four times throughout the two-year study period (*see "LTM" site locations in Figure S4*). To ensure precision, these measurements were taken in the channel adjacent to permanent infrastructure. Additional densiometer measurements were taken at all 49 sensor locations in the Piedmont research watershed once in June 2022. Each individual measurement consisted of averaging four to six canopy cover measurements within a stream reach, and canopy cover was calculated as the total number of covered quadrants within the densiometer divided by the total number of quadrants.

Using both temporally and spatially distributed densiometer measurements, relative proportions of vegetation types were calculated by comparing late-winter leaf-off measurements (i.e., a proxy for coniferous vegetation) to late-summer leaf-on measurements. For each location, the leaf-off measurements were subtracted from their respective leaf-on measurements to calculate relative proportion of deciduous vegetation. These calculations were then aggregated by HGF, and the percent of deciduous vegetation was calculated as the average ratio of deciduous vegetation to the total leaf-on measurement x 100. The percent of coniferous vegetation for each HGF was calculated as the average ratio of leaf-off measurement to leaf-on measurement x 100.

2.4 Statistical Analyses

To evaluate relationships and statistical significance between physiographic variables and water persistence, we first filtered the dataset to include only non-perennial sensors (i.e., sensors that recorded dry conditions at some point across the study period; $n = 13$ for the Piedmont watershed, $n = 19$ for the Appalachian Plateaus and Coastal Plain watersheds) for the 2024 water year. We selected the 2024 water year because this was the driest year of the study when all three watersheds experienced the shortest ASDN lengths and largest number of non-perennial sensors. Although we describe patterns across multiple years, we focus our hierarchical analysis of drivers solely on the 2024 water year for this reason. Most analyses were performed on this subset of data and were grouped by study watershed unless noted otherwise.

For the relationships between physiographic variables and water persistence, we performed individual correlation tests between each variable and water persistence using Spearman's rank correlation coefficient (ρ) to account for our non-parametric data. For within-watershed statistical testing, we aggregated the sensors into groups according to their HGFs (as noted above in Section 2.1). We then used a Kruskal-Wallis test to evaluate significance of each physiographic variable and water persistence across the groups. For significant relationships, we then performed a post hoc Dunn's test to evaluate which differences between pairwise groups were significant. For all statistical analyses, we assigned a significance level of $p < 0.05$.

To test the hierarchical relationship between all of our physiographic variables, we also used a random forest model to evaluate variable importance. We constructed four random forest

models – one model for each watershed, as well as one global model using data across all three watersheds – using the *randomForest* package in R (Liaw & Wiener, 2024). For each model, we first filtered out highly correlated predictor variables by calculating Spearman's rank correlation coefficient for every pair of potential variables and removing one variable from each pair with $\rho > 0.9$. We split our data into training and testing sets, randomly assigning 70% of our water persistence site observations to the training set and the other 30% to the testing set. We then used this final predictor variable and training dataset in the model and constructed the final model using 500 trees and 5 predictor variables at a time. We evaluated model performance by calculating Root Mean Squared Error (RMSE), coefficient of determination (R^2), Mean Absolute Error (MAE), and Mean Absolute Percent Error (MAPE) for both our training and testing datasets. Finally, we evaluated variable importance by calculating the percent increase in Mean Standard Error (incMSE%) for each variable when it was removed from the model.

3 Results

3.1 Direction and magnitude of network expansion and contraction varied across watersheds

Our three watersheds each had distinct spatial patterns in water persistence. In the Piedmont watershed, only 13 sites went dry at any point ($n = 20$ total sites), and these non-perennial locations were primarily concentrated in the headwaters of the network (Figure 3C). Nonetheless, the watershed outlet also experienced zero-flow during this period, but the mainstem and lower portions of the network did not dry. In the Coastal Plain, there was a higher proportion of non-perennial sites ($n = 19$), but they were similarly located furthest from the watershed outlet (Figure 3B). The only site to never go dry was in the most incised portion of the channel network. Moreover, incised regions in the middle of the network had higher water persistence than nearby un-incised reaches. In the Appalachian Plateaus, we observed unique patterns in network expansion and contraction. Here, the portions of the network with the lowest water persistence were closest to the outlet, suggesting bottom-up network contraction (Figure 3A). Similar to the Coastal Plain, the majority of the Appalachian Plateaus watershed dried ($n =$

19), but the sites with the highest water persistence were clustered together in the headwaters of this watershed where cave-springs have been observed in the highest density.

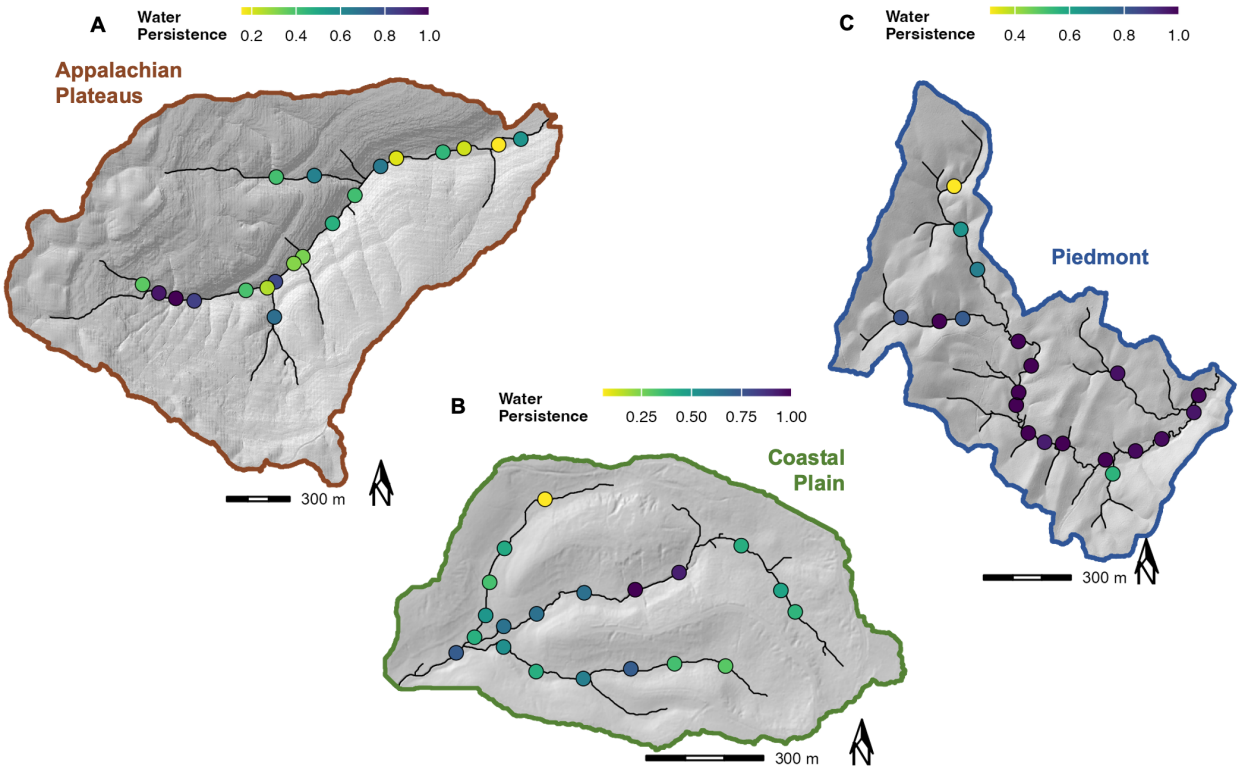

Figure 3. Spatial patterns in water persistence across the 2024 water year. Each point is an individual sensor colored by the proportion of the 2024 water year the sensor recorded wet conditions.

Across our three watersheds, we also observed seasonal patterns and interannual variability in network expansion and contraction. All three watersheds exhibited greater ASDN lengths in the winter and early spring (network expansion in late January through March; centered around day of water year ≃ 100), and lower ASDN lengths in the late summer and early fall (contraction and disconnection in August through early November; centered around day of water year ≃ 350; Figure 4). However, the exact timing of the start and peak of the annual drydown varied by watershed, with the Appalachian Plateaus generally starting to contract and reaching its lowest ASDN length earlier than the other watersheds, and the Piedmont contracting and reaching its lowest ASDN length the latest (Figure 4). Though the 2024 water year patterns were consistent with the 2023 water year for the Piedmont (Figure 4B), the drydown was slightly

earlier in the Appalachian Plateaus (Figure 4A) and Coastal Plain (Figure 4C) for the 2024 water year.

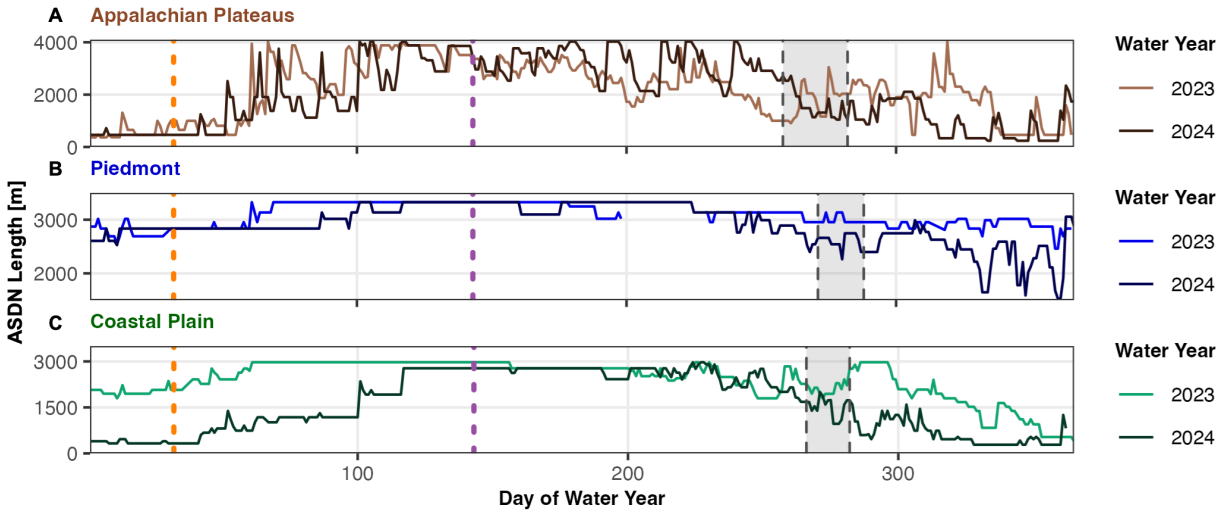

Figure 4. Active Surface Drainage Network (ASDN) length (m) throughout time, with the lighter color reflecting the 2023 water year, and the darker color reflecting the 2024 water year (where the water year begins Oct. 1). **(A)** is the Appalachian Plateaus watershed, **(B)** is the Piedmont watershed, and **(C)** is the Coastal Plain watershed. Periods of highest potential evapotranspiration (PET; defined as the 90th percentile of daily PET values at each site for the 2023 and 2024 water years) for each watershed are indicated in the grey shaded area (Peterson & Jones 2025d; 2025e; 2025g). Additionally, the start of the leaf-off period is indicated by the vertical orange dashed line (day of water year = 32), and the start of the leaf-on period is indicated by the purple dashed line (day of water year = 143). Leaf-on and leaf-off dates were determined based on field observations and records from the USA National Phenology Network (http://www.usanpn.org).

Further, we observed that the magnitude of network expansion and contraction differed across watersheds. The Appalachian Plateaus watershed had the greatest proportion of network contraction, shrinking from 100% (fully connected) in June 2024 to 6% of the potential network length in August 2024 (4,026 m to 238 m; Figure 4A). The Coastal Plain watershed also had a large magnitude of network contraction, going from 100% in May 2024 to 9% of the potential network length in August and September 2024 (2,972 m to 282 m; Figure 4C). Comparatively, the Piedmont watershed had minimal network contraction, only shrinking from 100% connected

in May 2024 to 43% of the potential network length in September 2024 (3,326 m to 1,417 m; Figure 4B). Further, the magnitude of network contraction varied between years, with 2024 yielding lower minimum network lengths for all three watersheds. Altogether, we observed that the Appalachian Plateaus and Coastal Plain were relatively dynamic watersheds that experienced large cycles of network expansion and contraction, whereas the Piedmont watershed was relatively stable and only experienced partial network contraction.

3.2 Physiographic drivers varied across watersheds

We found that at the watershed scale, topographic metrics were variably important to water persistence across physiographic regions. We compared our 2024 water persistence data for each watershed to three primary topographic drivers: drainage density as a proxy for convergence, slope of the channel, and curvature (Figure 5). We found that drainage density was positively correlated with water persistence for the Piedmont watershed ($\rho = 0.60$; Table 2), where higher flow convergence tended to yield greater water persistence, though this relationship was non-significant ($p = 0.22$; Figure 5A, Table 2). We found that stream slope was significantly related to water persistence in the Appalachian Plateaus ($\rho = 0.49$, $p = 0.01$) and the Piedmont ($\rho = -0.65$, $p < 0.01$; Table 2); however, the relationship was positive in the Appalachian Plateaus (i.e., steeper slopes related to greater water persistence) but negative in the Piedmont (i.e., shallower slopes related to greater water persistence; Figure 5B). Finally, we found greater curvature led to significantly higher water persistence in the Coastal Plain ($\rho = 0.46$, $p < 0.01$; Figure 5C, Table 2), but significantly lower water persistence in the Piedmont ($\rho = -0.48$, $p = 0.05$; Figure 5C, Table 2). Altogether, we found that water persistence in each watershed was significantly correlated to at least one, but not all three, of the primary topographic driver variables. Similarly, we found that no single variable was significantly correlated with water persistence variability in all three watersheds.

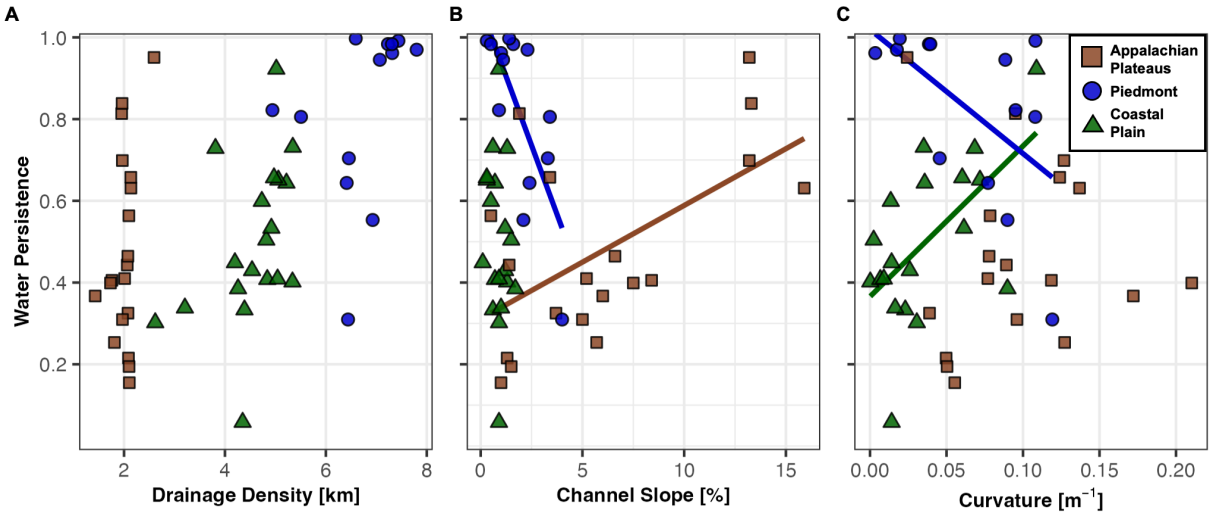

Figure 5. Relationships between site-specific annual water persistence and the three primary topography metrics: **(A)** drainage density as a proxy for flow convergence**, (B)** slope of the channel, and **(C)** curvature. Relationships with significant correlations (as noted in Table 2) are marked with solid lines. Colored points and lines correspond to the watersheds in this study, where brown is the Appalachian Plateaus, blue is the Piedmont, and green is the Coastal Plain (further indicated in the legend).

Further, we observed that while some topographic metrics were significantly correlated with water persistence for all three watersheds (e.g., TWI; see Table 2), the directionality of these relationships differed between watersheds. For example, the relationship between TWI and water persistence was positive in the Piedmont ($\rho = 0.58$) and Coastal Plain ($\rho = 0.51$), but negative for the Appalachian Plateaus ($\rho = -0.53$). Additionally, we found that several metrics that were significantly correlated with water persistence for each watershed strongly covaried; for example, distance to outlet, drainage area, and TWI are all calculated using the same area accumulation technique, and TWI was significantly correlated with water persistence across all three watersheds. Further, we found that there was a strong correlation and significant negative relationship between elevation and water persistence for the Piedmont watershed (i.e., higher elevations had lower water persistence; $\rho = -0.64$, $p < 0.01$; Table 2). Altogether, we expect that the relationships observed here likely reflect larger-scale watershed patterns, and thus may correlate with other physiographic drivers.

Table 2. *Spearman's Correlation Coefficients (ρ) and Statistical Significance for All Topographic Metrics*

Water Persistence ~	**Appalachian Plateaus**		**Piedmont**		**Coastal Plain**	
	ρ	**p-value**	**ρ**	**p-value**	**ρ**	**p-value**
Drainage density	*0.09*	*0.13*	***0.60***	*0.22*	*0.52*	*0.06*
Channel Slope	*0.49*	***0.01***	***-0.65***	***< 0.01***	*-0.25*	*0.45*
Curvature	*0.21*	*0.63*	*-0.48*	***0.05***	*0.46*	***< 0.01***
Elevation	0.41	0.06	**-0.64**	**< 0.01**	-0.39	0.13
Slope	0.54	0.06	**-0.63**	**< 0.01**	0.25	0.44
Buffer slope	0.52	**0.04**	**-0.61**	**0.02**	**0.64**	**< 0.01**
Distance to outlet	0.36	0.06	**-0.67**	**0.02**	-0.24	0.39
Drainage area	-0.37	0.07	**0.71**	**0.01**	**0.72**	**< 0.01**
TWI	-0.53	**0.03**	0.58	**< 0.01**	0.51	**0.02**
TPI	0.09	0.61	0.32	0.20	-0.49	**< 0.01**

Note: All statistics performed on the non-perennial sensors (Piedmont $n = 13$, Appalachian Plateaus and Coastal Plain $n = 19$). Variables in bold are strongly correlated ($\rho > 0.6$) or statistically significant ($p < 0.05$). The three italicized variables are proxies for the three primary topographic variables outlined in Prancevic & Kirchner (2019), see Section 2.3.1.

At the HGF scale, we observed that within-watershed patterns in water persistence were related to watershed physiographic variables (i.e., geologic, vegetative, and soil characteristics; *Table S1*). In the Appalachian Plateaus watershed, the downstream A2 HGF dried 16% more than A1, although this difference was not significant (Figure 6A). Similarly, there were significant differences in depth to bedrock ($p = 0.03$; Figure 6D) and all other soil and vegetation variables between the two Appalachian Plateaus HGFs. However, we expect that this is likely an artifact of the structure of our data, as the physical differences between groups were very small, and the data were tightly clustered due to the resolution of the soils map in this region. In the Piedmont watershed, the most-upstream P1 HGF was approximately 28% drier than the other two HGFs on average ($p = 0.05$; Figure 6B), but there was no significant difference between the P2 and P3 HGFs. This was also reflected in the other physiographic variables, where the P1 HGF

had significantly shallower depths to bedrock ($p < 0.01$), higher saturated hydraulic conductivities ($p < 0.01$), and greater percentages of coniferous vegetation (though this was not statistically significant; Figure 6E). In the Coastal Plain, the C1 and C2 HGFs were approximately 23% drier than the most-downstream and incised C3 HGF ($p = 0.03$, Figure 6C). Interestingly, there were no statistically significant relationships between HGF and any of our physiographic variables in this watershed, which we again attribute to the unequal distribution of HGFs.

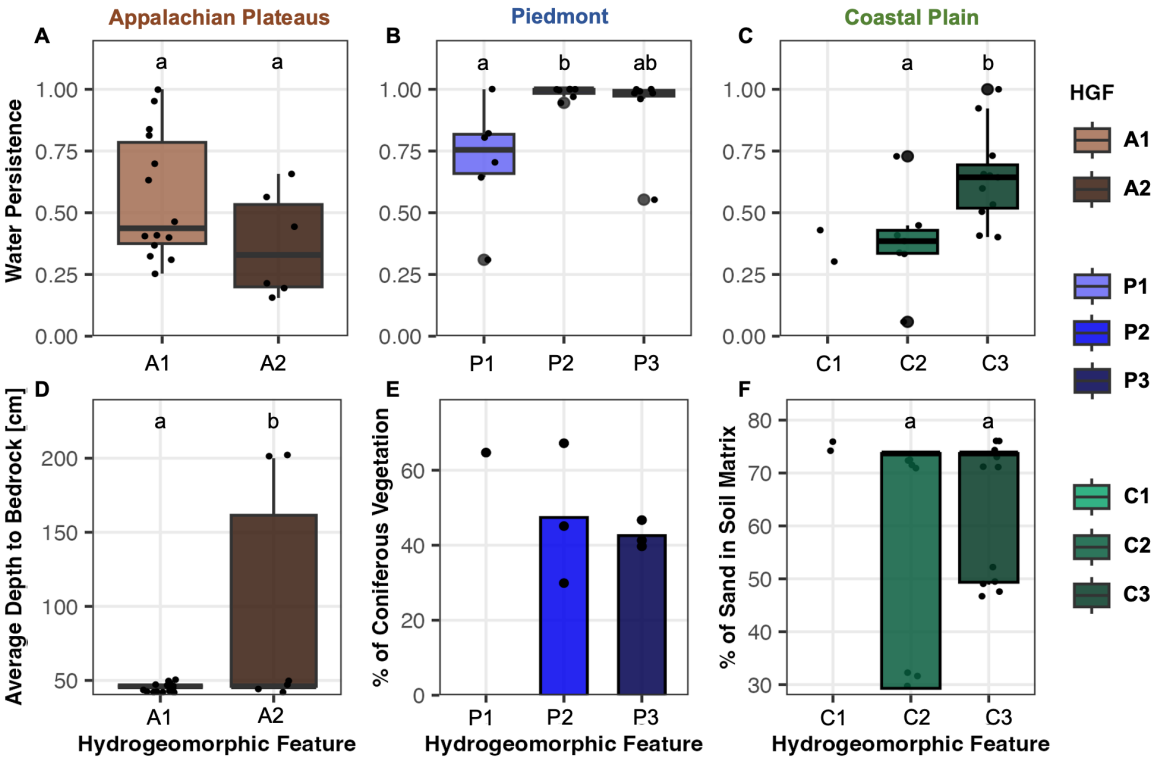

Figure 6. (A-C) Boxplots of water persistence across the HGFs for each watershed. **(D-F)** Plots of variables from all physiographic categories across the HGFs for each watershed. Significant differences between groups are denoted by letters above each group ($p < 0.05$). Analyses were performed on the entire dataset ($n = 20$ per watershed rather than the subsetted non-perennial data) for a more even distribution across groups, and groups with less than 6 observations were excluded from analyses. HGFs are ordered from most upstream to downstream. Panels **(D-F)** show variables from different physiographic categories: **(D)** depth to bedrock as a proxy for geologic features, **(E)** percent coniferous vegetation as a proxy for vegetative community

structure (n = 7, groups with less than 3 observations were excluded from mean calculations for the bars), and **(F)** percentage of sand in the soil matrix as a proxy for soil structure.

Using random forest models, we observed key differences in the topographic, vegetative, and soil-related drivers of water persistence across our three watersheds. Overall, individual watershed models performed better than the global model (*Table S4*). The Piedmont model was the most robust when evaluating our testing data (R^2 = 0.75) with minimal error (RMSE = 0.15, MAPE = 18.5; *Table S4*). The Coastal Plain model also performed well (R^2 = 0.56) with the lowest overall error parameters (*Table S4*). In contrast, the Appalachian Plateaus and global models performed relatively poorly (R^2 < 0.2, MAPE > 40; *Table S4*). As a result, we only evaluated variable importance for the Piedmont and Coastal Plain models where water persistence could be accurately predicted. When comparing variable importance, we observed generally low incMSE% values across all models (i.e., < 10%), suggesting that all variables were similarly important. In the Piedmont model, soil and vegetation properties were the two most important variables, though topographic variables also had relatively high importance (Figure 7A). Conversely, variables representing topographic drivers tended to be the most important in the Coastal Plain model, though there were several soil and vegetation parameters with positive incMSE% values (Figure 7B). However, no one variable was the most important in all models, suggesting varying local controls in flow persistence.

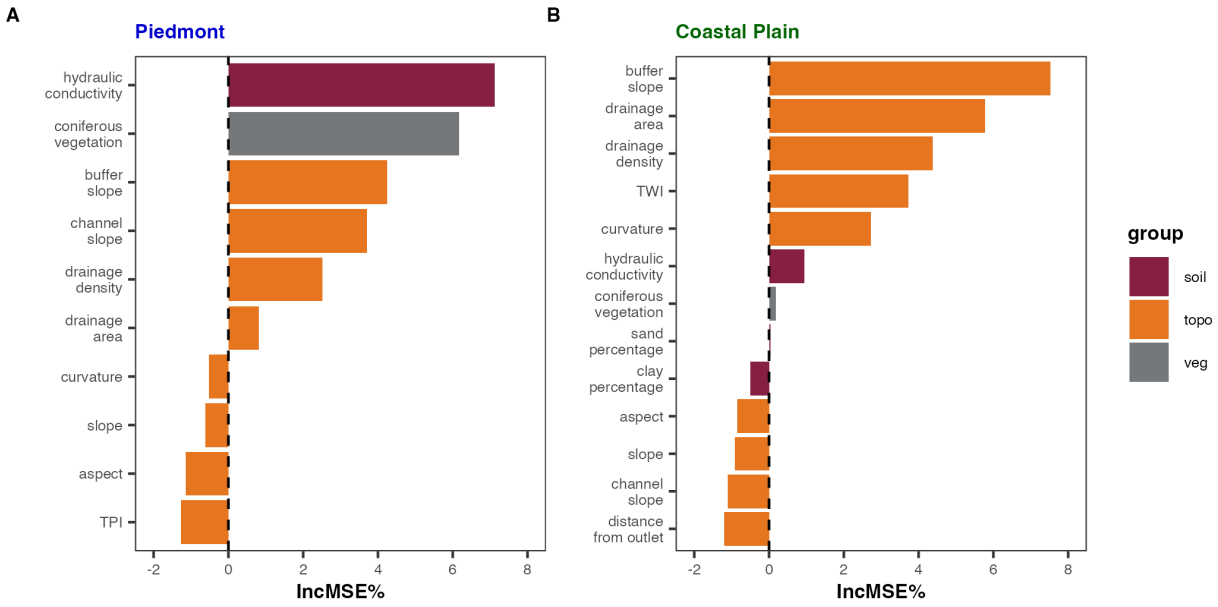

Figure 7. Results from the random forest models with accurate prediction of water persistence. We used a random forest model to investigate the relative importance (here, percent increase in mean standard error, incMSE%) of each of our variables to predicting water persistence at any given site. Variables are ordered from most to least important, and colored by physiographic category (i.e., soil, topography, or vegetation; geologic variables were removed due to high correlation with other variables). The Appalachian Plateaus watershed was omitted due to poor model performance.

3.3 Sensor placement influenced the results of network-scale expansion and contraction

When the more extensive sensor network was deployed in the Piedmont watershed from May 2022 through April 2023, there were key differences in the magnitude of network expansion and contraction, as well as the significant related drivers. Using only the 20 permanent sensors, the network appeared highly stable in the 2023 water year, with the smallest magnitude of network contraction across the three physiographic regions. However, when ASDN length was calculated using the high-density sensor network, the stream network was much more dynamic, expanding to 5,320 m during precipitation events, and contracting to 2,740 m during drydown (Figure 8A). Conversely, the permanent sensor network only captured a maximum expansion of 3,330 m and a minimum contraction of 2,540 m. Taken together, these results show that both sensor networks captured similar magnitudes of contraction during the drydown, but

the high-density network better captured expansion in the ephemeral headwater reaches of the network during precipitation events.

Further, we compared the relationships between the primary topographic drivers and site-specific water persistence using the high-density network. When considering the permanent network, there were significant correlations between water persistence for both slope and curvature (Figure 5), where steeper slopes and more concave valleys were significantly drier. However, we observed a different pattern when considering the high-density network. There was a significant positive correlation between drainage density and water persistence in the high-density network ($\rho = 0.73$, $p < 0.01$; Figure 8B), where increasing topographic convergence was correlated with increased water persistence. Similarly, there was a significant relationship between channel slope and water persistence in the high-density network (Figure 8C), with a highly negative correlation ($\rho = -0.79$) compared to a moderately negative correlation in the permanent network ($\rho = -0.65$). However, unlike the permanent network, the high-density network did not have a significant correlation between valley curvature and water persistence.

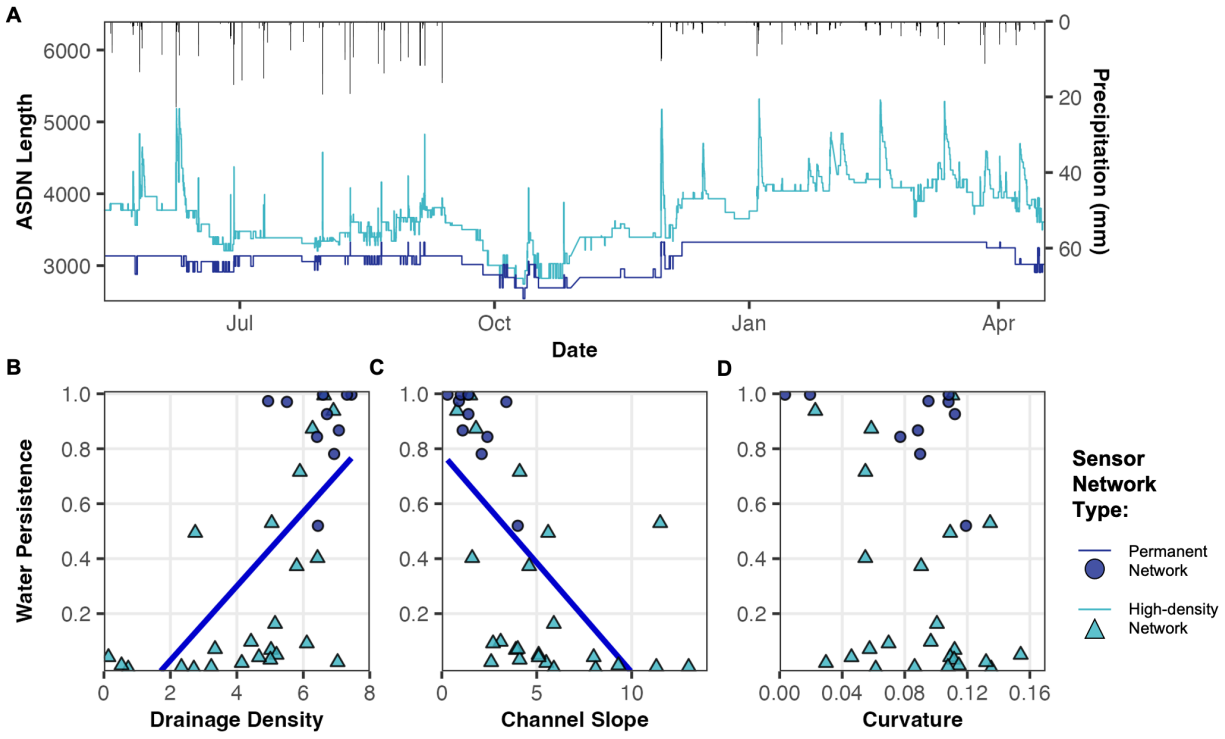

Figure 8. (A) ASDN length for the Piedmont research watershed as calculated from the permanent ($n = 20$) sensors in dark blue and from the high-density network ($n = 49$) in light blue,

with concurrent precipitation totals in black. **(B-D)** scatterplots of the relationships of our three primary topographic metrics when compared to the water persistence of all non-perennial STICs for this time period (n = 34 total; n = 10 in the permanent network, n = 24 in the high-density network).

3.4 Watersheds in the southeastern USA did not align with a topographic perceptual model of expansion and contraction

We compared the predicted relationship between discharge and network length with the measured relationship using the expansion exponent β (*sensu* Prancevic & Kirchner, 2019) to quantify how well topographic patterns explained network connectivity. The Piedmont watershed was the most comparable between the predicted and observed expansion exponent β (0.17 vs 0.08; Figure 9), though the model did predict the network to be more dynamic than we observed. However, there was poor agreement between the predicted and observed expansion exponent β for the Appalachian Plateaus and Coastal Plain watersheds. Using the topographic relationships, the Appalachian Plateaus watershed was predicted to be the most stable of the three (β = 0.04), while our results indicated the network was actually quite dynamic (0.19, Figure 9). Conversely, the Coastal Plain was predicted to be much more dynamic than observed (0.84 vs 0.13, Figure 9). Altogether, these results indicate that the topographic relationships derived in Prancevic & Kirchner (2019) did not represent observed network expansion and contraction in two of our three watersheds.

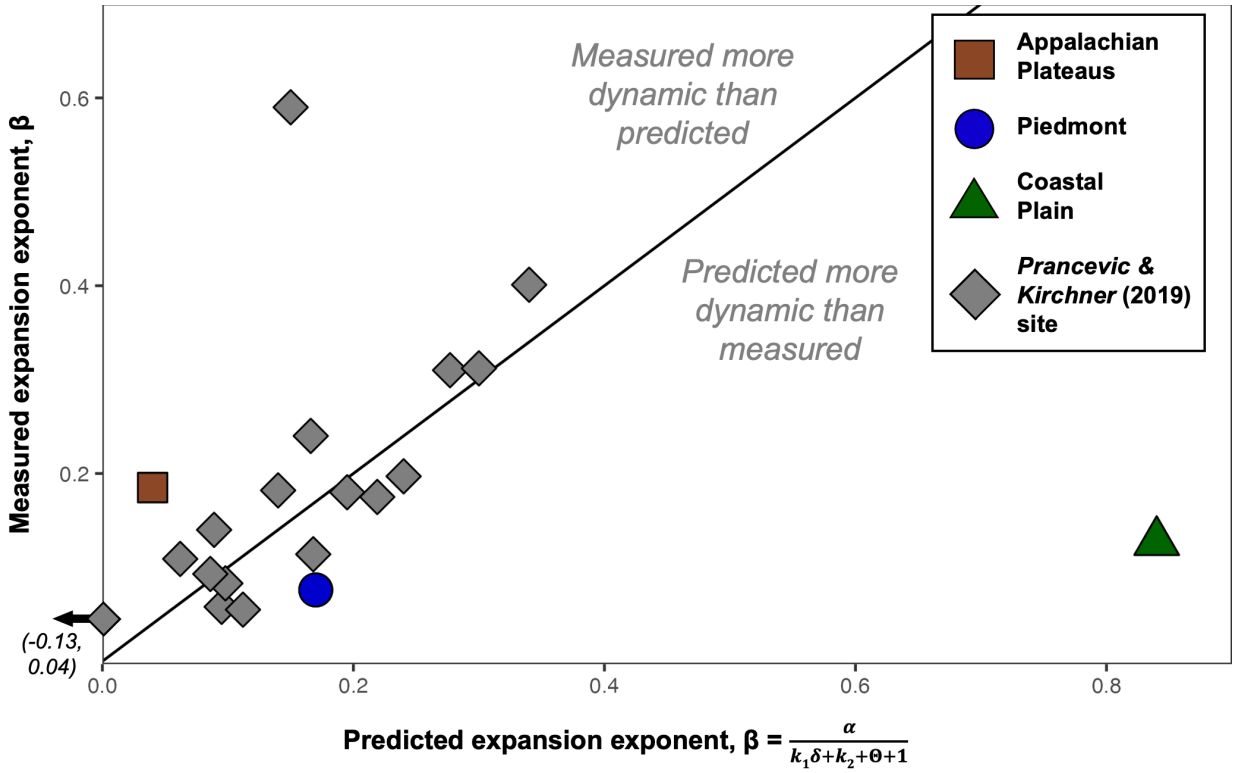

Figure 9. Relationships between predicted vs. observed expansion exponents with grey diamonds corresponding to observations from the original 17 watersheds used in Prancevic & Kirchner (2019). All points are relative to a 1:1 line, which represents perfect agreement between predicted and measured expansion exponents. Colored shapes correspond to the watersheds in this study.

4 Discussion

4.1 Relationships between topography and network expansion and contraction varied across and within our study watersheds in unexpected ways

Our study leveraged intensive monitoring of three watersheds in the southeastern USA to examine network-scale expansion and contraction as well as the drivers of water persistence within these same networks. Notably, our three watersheds had consistent precipitation patterns despite spanning a physiographic gradient, providing a natural experiment that allowed us to investigate the impacts of variables like topography, underlying geology, and vegetation on these network dynamics without the confounding controls of precipitation. Moreover, we are working in low-relief systems, which are underrepresented in contemporary perceptual models of network

dynamics. First, we examine how relationships between topographic variables and network expansion and contraction varied within watersheds. Then, to put our results into perspective with contemporary studies, we investigate the impact of topography by applying a topographic model developed by Prancevic & Kirchner (2019) across our three watersheds.

Within our three watersheds, the relationship between channel slope and water persistence was variable. While channel slope was significant for both the Piedmont and Appalachian Plateaus watersheds, it was positively correlated with water persistence in the Appalachian Plateaus, and negatively correlated in the Piedmont. Following the relationships between these topographic metrics and network expansion and contraction outlined by Prancevic & Kirchner (2019), we would expect a negative relationship, as decreasing slope would decrease subsurface flow, driving water to the surface and creating higher water persistence. Therefore, the Piedmont watershed aligned with this conceptualization, which has been supported by other studies (e.g., Montgomery & Dietrich, 1995; Rinderer et al., 2014). The Appalachian Plateaus demonstrated the opposite pattern, in which steeper slopes were correlated with wetter locations (see Section 4.2). While this is not the first study to find that topography does not fully explain network variability (e.g., Warix et al., 2021; Whiting & Godsey, 2016), our results suggest that low-relief watersheds do not align with these expected patterns because interactions between other controls, such as soil structure, underlying geology, and vegetative water demand (Figure 6), remain important drivers of network variability.

We found a similar pattern for curvature in the Coastal Plain and Piedmont watersheds. While valley curvature was significantly related to water persistence in both watersheds, it was positively correlated to water persistence in the Coastal Plain, and negatively correlated in the Piedmont. This also contradicts expectations; presuming that curvature is a proxy for valley transmissivity as a function of subsurface area and compressive forces (Prancevic & Kirchner 2019), we would expect higher curvature to relate to higher water persistence. Therefore, the Coastal Plain aligned with these expectations as well as with other studies (e.g., Kaplan et al., 2020). However, the Piedmont watershed demonstrated the opposite pattern, where greater curvatures were related to drier locations, which to our knowledge has not been documented in other networks. However, studies have found curvature to be an overall poor predictor of water

persistence in other networks (e.g., Warix et al., 2021), suggesting relatively complex interactions between valley curvature and streamflow permanence.

We also observed similar dynamics for TWI, which was one of the only significant metrics across all three watersheds. We observed the expected positive correlation between water persistence and TWI for both the Piedmont and the Coastal Plain, where higher TWIs were related with wetter portions of the network. However, the Appalachian Plateaus watershed demonstrated the opposite pattern, where portions of the network with higher TWIs were drier than other portions of the network. Given that TWI integrates both drainage area and slope (Beven & Kirkby, 1979), the Appalachian Plateaus watershed contradicts the assumption that larger areas paired with lower slopes yield wetter conditions. We anticipate that these unexpected patterns in topographic variables are more an expression of the bottom-up drying pattern we observed at this site (Figure 3). While the standard conceptualization is that networks expand and contract from the top-down (Biswal & Marani, 2010), our Appalachian Plateaus watershed disconnected at the outlet before contracting up-network, which has only been documented in a handful of other studies, often in more arid regions (e.g., Costigan et al., 2015; Senatore et al., 2021; Zipper et al., 2025). We expect these patterns are primarily caused by the geologic setting; the Appalachian Plateaus watershed is karst, and the majority of cave-springs and resulting locations of greatest flow persistence are located in the headwaters of this network, where contributing areas are small and slopes are steep. Overall, the varying importance of topography across these sites points to the importance of considering all components of physiography in low-relief networks: in the absence of clear topographic controls, the heterogeneity of otherwise subordinate controls becomes the more significant predictor of hydrologic dynamics.

Looking across watersheds and using the model developed by Prancevic & Kirchner (2019), we found relatively good agreement between the predicted and observed expansion exponents for our Piedmont watershed, but not for our Coastal Plain or Appalachian Plateaus watersheds (Figure 9). Notably, despite having the greatest similarity between predicted and observed expansion exponents, the observed β for the Piedmont watershed was among the lowest in the original study (0.08), indicating our Piedmont watershed has a relatively stable network. In contrast, while our Appalachian Plateaus watershed was predicted to have a similarly stable network ($\beta = 0.04$), we observed a more dynamic network ($\beta = 0.19$). Here, we expect that the

divergence between predicted and observed is related to the geologic heterogeneity within the watershed, similar to the patterns observed with TWI. Our Coastal Plain watershed was generally dynamic as well, though it had a higher predicted β than any of the original 17 watersheds (β = 0.84; Figure 9), which was much higher than the observed expansion exponent (β = 0.13). In part, this could be due to methodological differences in measurement of β (see Section 4.3). However, we expect that our Coastal Plain watershed represents an extrapolation beyond the range of landscapes captured by the original 17 watersheds in Prancevic & Kircher (2019). The Coastal Plain is a unique and diverse landscape, and this watershed is likely impacted by factors such as incision, land-use legacies, and unique channel forming factors associated with low-relief Coastal Plain landscapes (see Peterson et al., 2025). Taken together, these results indicate that topography alone is not able to accurately predict network expansion and contraction across our watersheds, suggesting that other potential drivers within are at play.

4.2 Watershed-scale patterns in connectivity are driven by interactions between topographic, geologic, and biotic variables

Hierarchical drivers are hypothesized to interact predictably across subordinate scales to drive emergent patterns of streamflow generation and network connectivity (McDonnell et al., 2007). At large spatial scales, there is general agreement that observable network-scale patterns in connectivity reflect and integrate hydroclimatic, geologic, and biologic conditions across both spatial and temporal scales (e.g., Godsey & Kirchner, 2014; Hynes, 1975; Newcomb & Godsey, 2023; Ward et al., 2018). Further, it has been well documented that variability in these conditions across space translates to watershed-scale variability in network connectivity (e.g., Jensen et al., 2017; Lovill et al., 2018). However, we do not yet have a clear and predictive understanding of the drivers of this network variability and the hierarchical interactions between them and across landscapes. For example, Hewlett & Hibbert (1967) observed that in a high-relief watershed in the Appalachian mountains, streamflow generation was controlled primarily by depth to an impervious layer, followed hierarchically by topography, climate, and land use. Other studies have documented meteorology and land use or land cover as key first-order controls on network connectivity across regions (e.g., Costigan et al., 2016; Hammond et al., 2021; Zipper et al.,

2021). Therefore, identifying the primary watershed-scale controls on network dynamics is challenging and often site-specific.

In this study, there was very consistent meteorology and land use across our study watersheds, yet we still observed significant differences in network connectivity (i.e., Figure 4; similar to the findings in Lovill et al., 2018). Therefore, these observed patterns must be due to other controls, which we expect may be differences in physiographic variables across these regions. Our data exhibit significant relationships between water persistence and a combination of soil, vegetation, and topographic characteristics in every watershed (e.g., Table 2, Figure 6). Further, we observed that across all three watersheds, variables from all physiographic categories were similarly significant in our random forest models, suggesting that topographic, geologic, and vegetative variables were all important to predicting water persistence (Figure 7).

While topography plays a large role in how water moves through watersheds (see Section 4.1), our data highlight the importance of considering other aspects of physiography across watersheds. For example, in the low relief of the Coastal Plain, our results paired with other studies suggest that where there are minimal slope changes that would normally drive flow to the surface, topographic convergence will instead drive flow generation (e.g., Montgomery & Dietrich, 1995). Additionally, the significant positive relationship between curvature and water persistence in the Coastal Plain likely reflects erosive and compressive processes that reduce downvalley flows and increase water persistence (Prancevic & Kirchner, 2019). Many studies have attributed this pattern in curvature and transmissivity to bedrock fracturing and weathering processes (e.g., Miller & Dunne, 1996; Moon et al., 2017). However, in our Coastal Plain watershed, where depths to bedrock are tens of meters deep, this pattern likely reflects the importance of stream incision and channel erosion in dictating flow generation and persistence in low-relief networks (e.g., Peterson et al., 2025). Figure 6C highlights that the highest water persistence values are found in the HGF characterized by channel incision, which can increase lateral connectivity from riparian water tables to the stream channel and sustain flows (Peterson et al., 2025; Kirker at al., 2025). Further, we anticipate that the significant relationships between slope and water persistence in the Piedmont reflects a decrease in slope that slows subsurface valley flow, resulting in subsurface water being forced to the surface (Prancevic et al., 2025).

Together, our research watersheds represent alternative ways that topographic variables can influence network expansion and contraction.

Our results also demonstrate the role underlying geology and resulting soil characteristics play in network connectivity. In the Appalachian Plateaus, reaches in the most upstream HGF were generally wetter than reaches in the downstream HGF (Figure 3, Figure 6A). In the uppermost HGFs, a combination of karst geologic formations and shallow soils likely explains increased flow persistence. These reaches are located in the outcropping of the Bangor limestone unit, which contains a high density of caves and karst formations (Ponta, 2018) that are likely persistent sources of deep groundwater (e.g., Hartmann et al., 2014). Moreover, reaches in the upstream HGF had relatively shallow soils (Figure 6D) and thus lower capacity for subsurface flow. In contrast, reaches in the valley bottom HGF experienced decreased flow persistence likely due to increased subsurface storage in alluvial deposits. As the valley transitioned to lower-gradient reaches dominated by alluvial deposits and increased subsurface storage (Figure 6D), subsurface capacity to transmit flow drastically increased, likely resulting in observed stream drying. Other studies have documented similar disconnectivities occurring within networks as a result of heterogeneity in subsurface structure (e.g., Glaser et al., 2025; Jensen et al., 2017; Whiting & Godsey, 2016), further reinforcing the role both geology and soil structure play within networks. These results are further supported by our observations in the Piedmont watershed, where the drier headwaters also had significantly shallower depths to bedrock and higher saturated hydraulic conductivities with coarser soil textures. These soil conditions likely increased transmissivity, which contributes to lower water persistence as water is moved downvalley more efficiently (Godsey & Kirchner, 2014). Together, these two watersheds highlight the role geologic setting plays in driving network connectivity.

In addition to the physical context of watersheds, our findings indicate that vegetative communities can contribute to network-scale patterns in connectivity both spatially and temporally. Since all three research watersheds were forested, we interpret the timing of network contraction in the late summer and early fall to be a function of vegetative water demand and transpiration during the peak growing season (Figure 4). The timing of network reconnection and expansion in the late fall and early winter coincides with leaf-off and vegetative dormancy, which reduces vegetative water demand (Figure 4). For example, Bergstrom et al. (2025)

observed that the timing and likelihood of stream drying was tied to seasonal climatic patterns like temperature, which when paired with water availability drives evapotranspiration. Taken with our results, these dynamics highlight that the timing of network drying in our watersheds is closely linked with the timing of plant productivity and water use. Additionally, we observed notable spatial patterns in vegetative community structure within our watersheds. For example, the vegetative community structure of the Piedmont watershed mirrored patterns in water persistence, in that there was more coniferous vegetation in the drier headwaters. The coniferous vegetation could result in both more consistent vegetative water demand throughout the year (Swank et al., 1989; Young-Robertson et al., 2016) and increases in interception that decrease infiltration and soil water recharge (Rutter at al., 1975). However, there are complex feedbacks between plant water use and water availability for streamflow (Bergstrom et al., 2025); for example, many coniferous species require well-drained, drier soils like those found in the headwaters of the Piedmont watershed. Taken together, the network connectivity in the Piedmont watershed is likely a function of feedbacks in vegetative water demand; the headwaters were increasingly drier as plant-water interactions reduced subsurface water storage. This aligns with other studies that have found that vegetative patterns influence connectivity at reach (Newcomb & Godsey, 2023, Warix et al., 2021) and network scales (e.g., Lee et al., 2020; Bergstrom et al., 2016). Altogether, the topographic, geologic, and vegetative context of these watersheds better explains the observed patterns within our networks than does topography alone.

4.3 Within-watershed patterns in connectivity are tied to the scales of observation

Despite our standardized site design, we found that placement of sensors affected our network-scale results. Generally, emergent watershed properties are based on the scales of observation, and so the patterns observed at one scale integrate all processes occurring at subordinate scales (McDonnell et al., 2007). Therefore, based on the established relationship between area accumulation and streamflow generation (e.g., Beven & Kirkby, 1979), we expected stream heads to occur at similar thresholds in similarly sized watersheds with consistent precipitation inputs (e.g., Montgomery & Dietrich, 1989). However, the results in our Coastal Plain and Piedmont watersheds did not support this conceptualization, with the transition from non-perennial to perennial flow occurring much higher in the network in the Piedmont than the Coastal Plain (Figure 3). We expect that this is likely a function of the geologic setting of these

watersheds; given the shallow and likely fractured bedrock of the Piedmont watershed, deep groundwater from fracture-flow likely contributed to streamflow in its headwaters (e.g., Boutt et al., 2010). This would generate more perennial flow higher in the network compared to the Coastal Plain, where flow persistence is likely driven by topographic convergence, soil properties, and channel incision (e.g., Gutiérrez-Jurado et al., 2019; Montgomery & Dietrich, 1995; Peterson et al., 2025).

Our results in the Piedmont watershed emphasize the importance of site selection and sensor distribution on network-scale patterns. We found that better capturing the non-perennial portions of our Piedmont network strengthened the relationships between water persistence and topographic metrics. However, of the three primary topographic metrics (i.e., drainage density, channel slope, and curvature, sensu Prancevic & Kirchner, 2019), only drainage density and channel slope were statistically significant predictors of water persistence in the permanent network (n = 20). Conversely, channel slope and curvature were the only statistically significant predictors of water persistence in the high-density network (n = 49). Therefore, while the significance of channel slope on water persistence increased with the higher density network, this was the only topographic metric that was significant in both sensor networks. Moreover, the high-density network captured a larger magnitude of network expansion and contraction, though this only marginally affected the generally low observed β.

We originally placed the permanent sensors based on the relationship between area accumulation and slope (*sensu* Zipper et al., 2025) without prior knowledge of the true dynamics of the system, which resulted in a bias towards lower, wetter portions of the network. While there is a precedent for distributing sensors randomly or evenly throughout a network to better capture a range of conditions (e.g., Jaeger & Olden, 2012; Jensen et al., 2019; Warix et al., 2021), this approach was less effective in our Piedmont watershed (due to the relatively small area accumulation thresholds). However, if our sensor design had considered the potential for fracture flow to occur higher in the network, we could have distributed the sensors across a more representative gradient of wetness conditions. Therefore, our study highlights the importance of considering more than just topographic conditions when designing and deploying sensor networks.

Moreover, our results highlight the importance of balancing both unbiased sensor distributions with an understanding of the dynamics of the system. It can be challenging to find an appropriate balance in previously unstudied locations and systems that are underrepresented in our perceptual models (e.g., low-relief watersheds). With that in mind, we suggest that future studies continue to integrate both empirical observations of network length with systematic sensor deployment strategies. Here, we used the topographically-based stratified distribution (i.e., Figure 2A) as an initial attempt to build a perceptual model of our systems. We then used our observations of network extent dynamics and the geomorphic channel from the first year of data collection (water year 2022; excluded from this study because of above-average precipitation) to update our understanding of the system, and distribute our high-density network to collect additional data in more dynamic portions of the network. Many other studies have used empirical observations of network extent at high spatial and lower temporal resolution (i.e., stream-walking; Whiting & Godsey, 2016, Durighetto et al., 2020). Other studies have used sensor networks to measure both water persistence and network-scale patterns at high temporal and lower spatial resolution (e.g., Zanetti et al., 2022). Studies that have used both stream-walking and sensor networks are limited, but suggest that patterns observed with sensor networks are representative of even highly dynamic networks (e.g., Jensen et al. 2019, Kindred, 2022). Altogether, we emphasize that there are tradeoffs and considerations related to empirical data collection in dynamic networks, and consideration of the spatial and temporal scales of interest should drive sensor network design and data collection efforts. Further, we suggest that future work focuses on both the integration of techniques and the collection of data in diverse landscapes to better inform our understanding of network patterns across systems.

5 Conclusions

We used a high-resolution sensor network to measure network connectivity in three watersheds spanning a physiographic gradient in the southeastern US. We used both empirical and geospatial data to investigate the drivers of network expansion and contraction through the lens of physiography (i.e., topography, geology, and biotic communities). We compared these results at both the watershed and site scales to identify key patterns in network connectivity. Our study found that the low-relief systems in the southeastern USA did not align with previous observations linking topography and network expansion and contraction patterns. When

comparing three primary topographic drivers (drainage density as a proxy for flow convergence, slope, and valley curvature), we found that no single driver explained the variability observed in all three watersheds; furthermore, no watershed had a significant relationship with all three topographic drivers. Previously derived relationships between topography and network connectivity overestimated the magnitude of expansion and contraction in two of our lower-relief watersheds. However, by integrating physiographic drivers (e.g., soil properties, geology, and plant communities), we could better explain the network patterns observed. Additionally, we found that the placement and number of sensors influenced the significance of topographic drivers. Altogether, our study demonstrates that physiography is a useful template that can serve as a starting point for developing predictive relationships between watershed characteristics and hydrologic processes.

Acknowledgments

The authors received support from the AIMS Project (funded by the National Science Foundation, Award Number 2019603), the University of Alabama Graduate School, and the Alabama Water Institute. The authors would like to thank the US Forest Service, the Weyerhaeuser Company, and private landowner John Gully for their management and support of the research watersheds. The authors would also like to thank Dr. Jami Nettles, Dr. Ashleigh Kirker, Helen Czech, Patience Knight, Lidia Molina Serpas, Justus King, Caroline Anscombe, Jacob Ackerman, Kevin Shaw, Jasmine Morejon, Stella Wilson, Dr. Vanessa Marshall, and many other friends and colleagues for their help with instrument maintenance, site management, and fieldwork. We also gratefully acknowledge Dr. Dana Lapides and two other anonymous reviewers for their feedback and suggestions to improve this manuscript. We also would like to thank Dr. Jeff Prancevic for his help and engagement with earlier versions of this manuscript. The authors declare no conflicts of interest relevant to this study.

Open Research

All data used in this study are available through CUAHSI HydroShare in the public AIMS Data group (https://www.hydroshare.org/group/247), and are cited in appropriate locations within the text and linked in the references below. Additional information about these and co-collected data can be found in Plont et al. (2025; https://doi.org/10.5194/essd-2025-559). Associated analyses and scripts can be accessed at: https://github.com/dmpeterson2/STIC_physiographic_analyses#

References

Alabama Historical Commission. (2002). The History of Agriculture in Alabama: A Historic Context. Retrieved from https://ahc.alabama.gov/architecturalprogramsPDFs/History%20of%20Agriculture%20in%20Alabama.pdf

Bergstrom, A., Jencso, K., & McGlynn, B. (2016). Spatiotemporal processes that contribute to hydrologic exchange between hillslopes, valley bottoms, and streams. Water Resources Research, 52(6), 4628–4645. https://doi.org/10.1002/2015WR017972

Bergstrom, A., Price, A. N., Beers, M., & Roche, K. R. (2025). Climate Forcings Across Multiple Timescales Control Stream Drying and Wetting in a Headwater Catchment. Hydrological Processes, 39(6), e70167. https://doi.org/10.1002/hyp.70167

Bernal, S., Lupon, A., Wollheim, W. M., Sabater, F., Poblador, S., & Martí, E. (2019). Supply, Demand, and In-Stream Retention of Dissolved Organic Carbon and Nitrate During Storms in Mediterranean Forested Headwater Streams. Frontiers in Environmental Science, 7. https://doi.org/10.3389/fenvs.2019.00060

Beven, K. J., & Kirkby, M. J. (1979). A physically based, variable contributing area model of basin hydrology / Un modèle à base physique de zone d'appel variable de l'hydrologie du bassin versant. Hydrological Sciences Bulletin, 24(1), 43–69. https://doi.org/10.1080/02626667909491834

Biswal, B., & Marani, M. (2010). Geomorphological origin of recession curves. Geophysical Research Letters, 37(24). https://doi.org/10.1029/2010GL045415

Botter, G., & Durighetto, N. (2020). The Stream Length Duration Curve: A Tool for Characterizing the Time Variability of the Flowing Stream Length. Water Resources Research, 56. https://doi.org/10.1029/2020WR027282

Botter, G., McNamara, J., & Durighetto, N. (2024). Extending Active Network Length Versus Catchment Discharge Relations to Temporarily Dry Outlets. Water Resources Research, 60(1), e2023WR035617. https://doi.org/10.1029/2023WR035617

Boutt, D. F., Diggins, P., & Mabee, S. (2010). A field study (Massachusetts, USA) of the factors controlling the depth of groundwater flow systems in crystalline fractured-rock terrain. Hydrogeology Journal, 18(8), 1839–1854. https://doi.org/10.1007/s10040-010-0640-y

Brinkerhoff, C. B., Gleason, C. J., Kotchen, M. J., Kysar, D. A., & Raymond, P. A. (2024). Ephemeral stream water contributions to United States drainage networks. Science, 384(6703), 1476–1482. https://doi.org/10.1126/science.adg9430

Burke, E., Wilhelm, J., Zipper, S., & Brown, C. (2024). AIMS SOP STIC Calibration. CUAHSI HydroShare. Retrieved from https://hydroshare.org/resource/9f2027c779d64149be32bdb9eede54f2/

Burt, T. P., & McDonnell, J. J. (2015). Whither field hydrology? The need for discovery science and outrageous hydrological hypotheses. Water Resources Research, 51(8), 5919–5928. https://doi.org/10.1002/2014WR016839

Busch, M. H., Costigan, K. H., Fritz, K. M., Datry, T., Krabbenhoft, C. A., Hammond, J. C., et al. (2020). What's in a Name? Patterns, Trends, and Suggestions for Defining Non-Perennial Rivers and Streams. Water, 12(7), 1980. https://doi.org/10.3390/w12071980

Chapin, T. P., Todd, A. S., & Zeigler, M. P. (2014). Robust, low-cost data loggers for stream temperature, flow intermittency, and relative conductivity monitoring. Water Resources Research, 50(8), 6542–6548. https://doi.org/10.1002/2013WR015158

Chescheir, G. M., Nettles, J. E., Youssef, M., Birgand, F., Amatya, D. M., Miller, D. A., et al. (2018). Optimization of Southeastern Forest Biomass Crop Production: A Watershed Scale Evaluation of the Sustainability and Productivity of Dedicated Energy Crop and Woody Biomass Operations (No. DOE-NCSU--04395). North Carolina State Univ., Raleigh, NC (United States). https://doi.org/10.2172/1437923

Cook, T. A. (1982). Stratigraphy and structure of the central Talladega slate belt, Alabama Appalachians. In D. N. Bearce, W. W. Black, S. A. Kish, & J. F. Tull (Eds.), Tectonic Studies in the Talladega and Carolina Slate Belts, Southern Appalachian Orogen (p. 0). Geological Society of America. https://doi.org/10.1130/SPE191-p47

Costigan, K. H., Daniels, M. D., & Dodds, W. K. (2015). Fundamental spatial and temporal disconnections in the hydrology of an intermittent prairie headwater network. Journal of Hydrology, 522, 305–316. https://doi.org/10.1016/j.jhydrol.2014.12.031

Costigan, K. H., Jaeger, K. L., Goss, C. W., Fritz, K. M., & Goebel, P. C. (2016). Understanding controls on flow permanence in intermittent rivers to aid ecological research: integrating meteorology, geology and land cover. Ecohydrology, 9(7), 1141–1153. https://doi.org/10.1002/eco.1712

Czikowsky, M. J., & Fitzjarrald, D. R. (2004). Evidence of Seasonal Changes in Evapotranspiration in Eastern U.S. Hydrological Records. Retrieved from https://journals.ametsoc.org/view/journals/hydr/5/5/1525-7541_2004_005_0974_eoscie_2_0_co_2.xml

Datry, T., Boulton, A. J., Bonada, N., Fritz, K., Leigh, C., Sauquet, E., et al. (2018). Flow intermittence and ecosystem services in rivers of the Anthropocene. The Journal of Applied Ecology, 55(1), 353–364. https://doi.org/10.1111/1365-2664.12941

Dobbs, N. A. (2016). Hydrology and Water Quality Dynamics in Coastal Plain and Upland Watersheds with Loblolly Pine (Pinus taeda) and Switchgrass (Panicum virgatum) Intercropping in the southeastern United States. Retrieved from http://www.lib.ncsu.edu/resolver/1840.20/33346

Dohman, J. M., Godsey, S. E., & Hale, R. L. (2021). Three-Dimensional Subsurface Flow Path Controls on Flow Permanence. Water Resources Research, 57(10), e2020WR028270. https://doi.org/10.1029/2020WR028270

Durighetto, N., Vingiani, F., Bertassello, L. E., Camporese, M., & Botter, G. (2020). Intraseasonal Drainage Network Dynamics in a Headwater Catchment of the Italian Alps. Water Resources Research, 56(4), e2019WR025563. https://doi.org/10.1029/2019WR025563

Feminella, J. W. (1996). Comparison of Benthic Macroinvertebrate Assemblages in Small Streams along a Gradient of Flow Permanence. Journal of the North American Benthological Society, 15(4), 651–669. https://doi.org/10.2307/1467814

Fenneman, N. M. (1938). Physiography of eastern United States. McGraw-Hill Book Company, inc. Retrieved from http://archive.org/details/physiographyofea0000nevi

Fickle, J. (2014). Green Gold. Retrieved June 20, 2025, from https://www.uapress.ua.edu/9780817318130/green-gold/

Florinsky, I. V. (2016). Chapter 1 - Digital Terrain Modeling: A Brief Historical Overview. In I. V. Florinsky (Ed.), Digital Terrain Analysis in Soil Science and Geology (Second Edition) (pp. 1–4). Academic Press. https://doi.org/10.1016/B978-0-12-804632-6.00001-8

Glaser, C., Gannon, J. P., Godsey, S. E., Grande, E., & Klaus, J. (2025). Streamflow (De)generation—How Do Streams Lose Flow? Hydrological Processes, 39(10), e70258. https://doi.org/10.1002/hyp.70258

Godsey, S., Wheeler, C., & Zipper, S. (2024). AIMS SOP STIC Deployment and Maintenance | CUAHSI HydroShare. CUAHSI HydroShare. Retrieved from https://hydroshare.org/resource/c82a87a6c63445029d35131260241386/

Godsey, S. E., & Kirchner, J. W. (2014). Dynamic, discontinuous stream networks: hydrologically driven variations in active drainage density, flowing channels and stream order. Hydrological Processes, 28(23), 5791–5803. https://doi.org/10.1002/hyp.10310

Golden, H. E., Christensen, J. R., McMillan, H. K., Kelleher, C. A., Lane, C. R., Husic, A., et al. (2025). Advancing the science of headwater streamflow for global water protection. Nature Water, 1–11. https://doi.org/10.1038/s44221-024-00351-1

Gómez-Gener, L., Siebers, A. R., Arce, M. I., Arnon, S., Bernal, S., Bolpagni, R., et al. (2021). Towards an improved understanding of biogeochemical processes across surface-groundwater interactions in intermittent rivers and ephemeral streams. Earth-Science Reviews, 220, 103724. https://doi.org/10.1016/j.earscirev.2021.103724

Griffith, G. E., Omernik, J. M., Comstock, J. A., Lawrence, S., Martin, G., Goddard, A., et al. (2001). Ecoregions of Alabama. U.S. Environmental Protection Agency, National Health and Environmental Effects Research Laboratory, Corvallis, OR.

Gutiérrez-Jurado, K. Y., Partington, D., Batelaan, O., Cook, P., & Shanafield, M. (2019). What Triggers Streamflow for Intermittent Rivers and Ephemeral Streams in Low-Gradient Catchments in Mediterranean Climates. Water Resources Research, 55(11), 9926–9946. https://doi.org/10.1029/2019WR025041

Hammond, J. C., Zimmer, M., Shanafield, M., Kaiser, K., Godsey, S. E., Mims, M. C., et al. (2021). Spatial patterns and drivers of non-perennial flow regimes in the contiguous U.S. Geophysical Research Letters, n/a(n/a), 2020GL090794. https://doi.org/10.1029/2020GL090794

Hartmann, A., Goldscheider, N., Wagener, T., Lange, J., & Weiler, M. (2014). Karst water resources in a changing world: Review of hydrological modeling approaches. Reviews of Geophysics, 52(3), 218–242. https://doi.org/10.1002/2013RG000443

Harvey, J., & Gooseff, M. (2015). River corridor science: Hydrologic exchange and ecological consequences from bedforms to basins. Water Resources Research, 51(9), 6893–6922. https://doi.org/10.1002/2015WR017617

Hewlett, J., & Hibbert, A. (1967). Factors Affecting the Response of Small Watersheds to Precipitation in Humid Areas. In Proceedings of the International Symposium on Forest Hydrology. Pergamon, Pennsylvania State University, NY.

Hollister, J.W. (2023). elevatr: Access Elevation Data from Various APIs (Version 0.99.0). Retrieved from https://CRAN.R-project.org/package=elevatr/

Hupp, C. (2000). Hydrology, Geomorphology and Vegetation of Coastal Plain Rivers in the South-Eastern USA. Hydrological Sciences, 14, 2991–3010. https://doi.org/10.1002/1099-1085(200011/12)14:16/17%3C2991::AID-HYP131%3E3.0.CO;2-H

Hynes, H. B. N. (1975). The stream and its valley. SIL Proceedings, 1922-2010, 19(1), 1–15. https://doi.org/10.1080/03680770.1974.11896033

Ilich, A., Lecours, V., Misiuk, B., & Murawski, S. (2025). MultiscaleDTM: Multi-Scale Geomorphometric Terrain Attributes (Version 1.0). Retrieved from https://cran.r-project.org/web/packages/MultiscaleDTM/index.html

Jaeger, K. L., & Olden, J. D. (2012). Electrical Resistance Sensor Arrays as a Means to Quantify Longitudinal Connectivity of Rivers. River Research and Applications, 28(10), 1843–1852. https://doi.org/10.1002/rra.1554

Jensen, C. K., McGuire, K. J., & Prince, P. S. (2017). Headwater stream length dynamics across four physiographic provinces of the Appalachian Highlands. Hydrological Processes, 31(19), 3350–3363. https://doi.org/10.1002/hyp.11259

Jensen, C. K., McGuire, K. J., McLaughlin, D. L., & Scott, D. T. (2019). Quantifying spatiotemporal variation in headwater stream length using flow intermittency sensors. Environmental Monitoring and Assessment, 191(4), 226. https://doi.org/10.1007/s10661-019-7373-8

Jones, C. N., Nelson, N. G., & Smith, L. L. (2019). Featured Collection Introduction: The Emerging Science of Aquatic System Connectivity I. JAWRA Journal of the American Water Resources Association, 55(2), 287–293. https://doi.org/10.1111/1752-1688.12739

Kaplan, N. H., Blume, T., & Weiler, M. (2020). Predicting probabilities of streamflow intermittency across a temperate mesoscale catchment. Hydrology and Earth System Sciences, 24(11), 5453–5472. https://doi.org/10.5194/hess-24-5453-2020

Kidd, R. E., & Lambeth, D. S. (1995). HYDROGEOLOGY AND GROUND-WATER QUALITY IN THE BLACK BELT AREA OF WEST-CENTRAL ALABAMA, AND ESTIMATED WATER USE FOR AQUACULTURE, 1990 (Water-Resources Investigations Report No. 94–4074). Tuscaloosa, Alabama: U.S. Geological Survey. Retrieved from https://web.archive.org/web/20190501065314id_/https://pubs.usgs.gov/wri/1994/4074/report.pdf

Kindred, T. (2022). Spatial Structure, Temporal Patterns, and Drivers of Stream Drying In the Gibson Jack Watershed, Bannock County, Idaho. Idaho State University, Pocatello, ID.

Kirker, A., Jones, C. N., Peterson, D. M., Tatariw, C., Nettles, J., & Chen, X. (2025). Storage, Connectivity, and Stream Drying in Headwater Systems: Modeling Across Hydrogeomorphic Features. Retrieved from https://www.authorea.com/doi/full/10.22541/essoar.175330904.43292818?commit=4f1b73625bde97ee589993712b5cb42733c86482

Kopaska-Merkel, D. C., Dean, L. S., & Moore, J. D. (2000). HYDROGEOLOGY AND VULNERABILITY TO CONTAMINATION OF MAJOR AQUIFERS IN ALABAMA: AREA 5.

Lee, S., McCarty, G. W., Moglen, G. E., Lang, M. W., Nathan Jones, C., Palmer, M., et al. (2020). Seasonal drivers of geographically isolated wetland hydrology in a low-gradient, Coastal Plain landscape. Journal of Hydrology, 583, 124608. https://doi.org/10.1016/j.jhydrol.2020.124608

Liaw, A., & Wiener, M. (2024). randomForest: Breiman and Cutlers Random Forests for Classification and Regression (Version 4.7-1.2). Retrieved from https://cran.r-project.org/web/packages/randomForest/index.html

Lindsay, J. B. (2016). Whitebox GAT: A case study in geomorphometric analysis. Computers & Geosciences, 95, 75–84. https://doi.org/10.1016/j.cageo.2016.07.003

Lovill, S. M., Hahm, W. J., & Dietrich, W. E. (2018). Drainage from the Critical Zone: Lithologic Controls on the Persistence and Spatial Extent of Wetted Channels during the

Summer Dry Season. Water Resources Research, 54(8), 5702–5726. https://doi.org/10.1029/2017WR021903

McDonnell, J. J., Sivapalan, M., Vaché, K., Dunn, S., Grant, G., Haggerty, R., et al. (2007). Moving beyond heterogeneity and process complexity: A new vision for watershed hydrology. Water Resources Research, 43(7). https://doi.org/10.1029/2006WR005467

McMillan, H., Araki, R., Gnann, S., Woods, R., & Wagener, T. (2023). How do hydrologists perceive watersheds? A survey and analysis of perceptual model figures for experimental watersheds. Hydrological Processes, 37(3), e14845. https://doi.org/10.1002/hyp.14845

Messager, M. L., Lehner, B., Cockburn, C., Lamouroux, N., Pella, H., Snelder, T., et al. (2021). Global prevalence of non-perennial rivers and streams. Nature, 594(7863), 391–397. https://doi.org/10.1038/s41586-021-03565-5

Miller, C. F., Hatcher, R. D., Ayers, J. C., Coath, C. D., & Harrison, T. M. (2000). Age and zircon inheritance of eastern Blue Ridge plutons, southwestern North Carolina and northeastern Georgia, with implications for magma history and evolution of the southern Appalachian orogen. American Journal of Science, 300, 142–172.

Miller, D. J., & Dunne, T. (1996). Topographic perturbations of regional stresses and consequent bedrock fracturing. Journal of Geophysical Research: Solid Earth, 101(B11), 25523–25536. https://doi.org/10.1029/96JB02531

Montgomery, D. R., & Dietrich, W. E. (1989). Source areas, drainage density, and channel initiation. Water Resources Research, 25(8), 1907–1918. https://doi.org/10.1029/WR025i008p01907

Montgomery, D. R., & Dietrich, W. E. (1995). Hydrologic Processes in a Low-Gradient Source Area. Water Resources Research, 31(1), 1–10. https://doi.org/10.1029/94WR02270

Moon, S., Perron, J. T., Martel, S. J., Holbrook, W. S., & St. Clair, J. (2017). A model of three-dimensional topographic stresses with implications for bedrock fractures, surface processes, and landscape evolution. Journal of Geophysical Research: Earth Surface, 122(4), 823–846. https://doi.org/10.1002/2016JF004155

Newcomb, S. K., & Godsey, S. E. (2023). Nonlinear Riparian Interactions Drive Changes in Headwater Streamflow. Water Resources Research, 59(10), e2023WR034870. https://doi.org/10.1029/2023WR034870

NOAA National Centers for Environmental Information. (2025). Climate at a Glance: County Time Series [Data set]. Retrieved from https://www.ncei.noaa.gov/access/monitoring/climate-at-a-glance/county/time-series

Peterson, D., N. Jones (2025a). Paint Rock Environmental Data (AIMS_SE_PRF_ENVI), HydroShare, http://www.hydroshare.org/resource/656211b1a1484433a3bc524fb968b4bd

Peterson, D., N. Jones (2025b). Shambley Creek Environmental Data (AIMS_SE_WHR_ENVI), HydroShare, http://www.hydroshare.org/resource/126d2c7b1c8d4889a8ccc454d387b0d8

Peterson, D., N. Jones (2025c). Talladega Environmental Data (AIMS_SE_TAL_ENVI), HydroShare, http://www.hydroshare.org/resource/81c003a7b8474d63a31641a4f375fd18

Peterson, D., N. Jones (2025d). Paint Rock Meteorological Data (AIMS_SE_PRF_approach1_METS), HydroShare, http://www.hydroshare.org/resource/4089918c0a494bfeb19be0421a33d297

Peterson, D., N. Jones (2025e). Shambley Creek Meteorological Data (AIMS_SE_WHR_approach1_METS), HydroShare, http://www.hydroshare.org/resource/33823d8603ce439fbba48fbcbba22da4

Peterson, D., N. Jones (2025f). Talladega Meteorological Data (AIMS_SE_TAL_approach1_METS), HydroShare, http://www.hydroshare.org/resource/281cd7627629481dbdc7d4ccf6fcfbcc

Peterson, D., N. Jones (2025g). Paint Rock Stream Temperature, Intermittency, and Conductivity Data (AIMS_SE_PRF_approach1_STIC), HydroShare, http://www.hydroshare.org/resource/d57338ebfb0240f58e8de37ddacf9426

Peterson, D., N. Jones (2025h). Shambley Creek Stream Temperature, Intermittency, and Conductivity Data (AIMS_SE_WHR_approach1_STIC), HydroShare, http://www.hydroshare.org/resource/dc623510ed1847f8abe1275904472c44

Peterson, D., N. Jones (2025i). Talladega Stream Temperature, Intermittency, and Conductivity Data (AIMS_SE_TAL_approach1_STIC), HydroShare, http://www.hydroshare.org/resource/ff306bec9fb24e52aa809dbb4d074731

Peterson, D. M., Jones, C. N., Plattner, A. M., Shogren, A. J., & Godsey, S. E. (2025). Using Hydrogeomorphic Features to Quantify Structural and Functional Hydrologic Connectivity in a Coastal Plain Headwater Stream. Water Resources Research, 61(8), e2024WR038533. https://doi.org/10.1029/2024WR038533

Plont, S., Peterson, D. M., Smith, C. R., Bond, C. T., Tchamba, A. L. K., Wolford, M. A., et al. (2025). Hydrologic, biogeochemical, microbial, and macroinvertebrate responses to network expansion, contraction, and disconnection across headwater stream networks with distinct physiography in Alabama, USA. Earth System Science Data Discussions, 1–40. https://doi.org/10.5194/essd-2025-559

Plont, S., S. Speir, D. Peterson, N. Jones (2025a). AIMS Paint Rock Continuous Discharge at Watershed Outlet Data (AIMS_SE_PRF_DISC), HydroShare, http://www.hydroshare.org/resource/043fc07f0c3b47bcabbd0bf5600d929f

Plont, S., S. Speir, D. Peterson, N. Jones (2025b). AIMS Shambley Creek Continuous Discharge at Watershed Outlet Data (AIMS_SE_WHR_DISC), HydroShare, http://www.hydroshare.org/resource/535797126b134ceaab9838df0ca00885

Plont, S., M. Wolford, K. Zarek, D. Peterson, N. Jones, S. Speir (2025). AIMS Talladega Continuous Discharge at Watershed Outlet Data (AIMS_SE_TAL_DISC), HydroShare, http://www.hydroshare.org/resource/fc7ae2d28e3c481d805902a79af90a95

Ponta, G. (2018). Geologic Framework of Karst Aquifer Systems in Alabama. Sinkhole Conference 2018. Retrieved from https://digitalcommons.usf.edu/sinkhole_2018/ProceedingswithProgram/Appalachian_Karst/6

Prancevic, J. P., & Kirchner, J. W. (2019). Topographic Controls on the Extension and Retraction of Flowing Streams. Geophysical Research Letters, 46(4), 2084–2092. https://doi.org/10.1029/2018GL081799

Prancevic, J. P., Seybold, H., & Kirchner, J. W. (2025). Variability of flowing stream network length across the US. Science, 387(6735), 782–786. https://doi.org/10.1126/science.ado2860

Pringle, C. M. (2001). Hydrologic Connectivity and the Management of Biological Reserves: A Global Perspective. Ecological Applications, 11(4), 981–998. https://doi.org/10.1890/1051-0761(2001)011[0981:HCATMO]2.0.CO;2

R Core Team. (2024). R: A Language and Environment for Statistical Computing. Vienna, Austria: R Foundation for Statistical Computing. Retrieved from https://www.R-project.org/

Rinderer, M., van Meerveld, H. J., & Seibert, J. (2014). Topographic controls on shallow groundwater levels in a steep, prealpine catchment: When are the TWI assumptions valid? Water Resources Research, 50(7), 6067–6080. https://doi.org/10.1002/2013WR015009

Rinderer, M., Ali, G., & Larsen, L. G. (2018). Assessing structural, functional and effective hydrologic connectivity with brain neuroscience methods: State-of-the-art and research directions. Earth-Science Reviews, 178, 29–47. https://doi.org/10.1016/j.earscirev.2018.01.009

Roberts, M., & Klingeman, P. (1972). The relationship of drainage net fluctuation and discharge. Proc. Internat. Geographical Congress, 181–191.

Rutter, A. J., Morton, A. J., & Robins, P. C. (1975). A Predictive Model of Rainfall Interception in Forests. II. Generalization of the Model and Comparison with Observations in Some Coniferous and Hardwood Stands. Journal of Applied Ecology, 12(1), 367–380. https://doi.org/10.2307/2401739

Sapp, C. D., & Emplaincourt, J. (1975). Physiographic regions of Alabama. Geological Survey of Alabama. Retrieved from https://ngmdb.usgs.gov/Prodesc/proddesc_55813.htm

Senatore, A., Micieli, M., Liotti, A., Durighetto, N., Mendicino, G., & Botter, G. (2021). Monitoring and Modeling Drainage Network Contraction and Dry Down in Mediterranean Headwater Catchments. Water Resources Research, 57(6), e2020WR028741. https://doi.org/10.1029/2020WR028741

Shaw, S. B. (2016). Investigating the linkage between streamflow recession rates and channel network contraction in a mesoscale catchment in New York state. Hydrological Processes, 30(3), 479–492. https://doi.org/10.1002/hyp.10626

Soil Survey Staff, Natural Resources Conservation Service, USDA. Accessed March 2025. Web Soil Survey [Data set]. Retrieved from https://websoilsurvey.nrcs.usda.gov/app/

Swenson, G. A. (1954). Soil Survey of Jackson County, Alabama. U.S. Department of Agriculture, Soil Conservation Service.

Swenson, L. J., Zipper, S., Peterson, D. M., Jones, C. N., Burgin, A. J., Seybold, E., et al. (2024). Changes in Water Age During Dry-Down of a Non-Perennial Stream. Water Resources Research, 60(1), e2023WR034623. https://doi.org/10.1029/2023WR034623

Swank, W., DeBano, L., & Nelson, D. (1989). Effects of Timber Management Practices on Soil and Water. In The Scientific Basis for Silvicultural and Management Decisions in the National Forest System. U.S. Department of Agriculture, Forest Service.

Szabo, E. W., Osborne, W. E., Copeland, C. W., & Neathery, T. L. (1988). Geologic map of Alabama. Geological Survey of Alabama. Retrieved from https://ngmdb.usgs.gov/Prodesc/proddesc_55859.htm

Trimble, S. W. (2008). Man-Induced Soil Erosion on the Piedmont, 1700-1970 (2nd ed.). Ankeny, IA: Soil and Water Conservation Society.

Wahl, K. D. (1966). Geology and ground-water resources of Greene County, Alabama. Geological Survey of Alabama. Retrieved from https://ngmdb.usgs.gov/Prodesc/proddesc_55588.htm

Wang, J.-P., François, B., & Lambert, P. (2017). Equations for hydraulic conductivity estimation from particle size distribution: A dimensional analysis. Water Resources Research, 53(9), 8127–8134. https://doi.org/10.1002/2017WR020888

Ward, A. S., Schmadel, N. M., & Wondzell, S. M. (2018). Simulation of dynamic expansion, contraction, and connectivity in a mountain stream network. Advances in Water Resources, 114, 64–82. https://doi.org/10.1016/j.advwatres.2018.01.018

Ward, J. V. (1989). The Four-Dimensional Nature of Lotic Ecosystems. Journal of the North American Benthological Society, 8(1), 2–8. https://doi.org/10.2307/1467397

Warix, S. R., Navarre-Sitchler, A., Manning, A. H., & Singha, K. (2023). Local Topography and Streambed Hydraulic Conductivity Influence Riparian Groundwater Age and Groundwater-Surface Water Connection. Water Resources Research, 59(9), e2023WR035044. https://doi.org/10.1029/2023WR035044

Warix, S. R., Godsey, S. E., Lohse, K. A., & Hale, R. L. (2021). Influence of groundwater and topography on stream drying in semi-arid headwater streams. Hydrological Processes, 35(5), e14185. https://doi.org/10.1002/hyp.14185

Whiting, J. A., & Godsey, S. E. (2016). Discontinuous headwater stream networks with stable flowheads, Salmon River basin, Idaho. Hydrological Processes, 30(13), 2305–2316. https://doi.org/10.1002/hyp.10790

Wilson, J. (2018). Calculating Land Surface Parameters. In Environmental Applications of Digital Terrain Modeling (pp. 53–149). John Wiley & Sons, Ltd. https://doi.org/10.1002/9781118938188.ch3

Wu, Q., & Brown, A. (2022). whitebox: "WhiteboxTools" R Frontend. R package version 2.2.0. Retrieved from https://CRAN.R-project.org/package=whitebox

Young-Robertson, J. M., Bolton, W. R., Bhatt, U. S., Cristóbal, J., & Thoman, R. (2016). Deciduous trees are a large and overlooked sink for snowmelt water in the boreal forest. Scientific Reports, 6(1), 29504. https://doi.org/10.1038/srep29504

Zanetti, F., Botter, G., & Camporese, M. (2024). Stream Network Dynamics of Non-Perennial Rivers: Insights From Integrated Surface-Subsurface Hydrological Modeling of Two Virtual Catchments. Water Resources Research, 60(2), e2023WR035631. https://doi.org/10.1029/2023WR035631

Zanetti, F., Durighetto, N., Vingiani, F., & Botter, G. (2022). Technical note: Analyzing river network dynamics and the active length–discharge relationship using water presence sensors. Hydrology and Earth System Sciences, 26(13), 3497–3516. https://doi.org/10.5194/hess-26-3497-2022

Zarek, K., Jones, C. N., Peterson, D. M., Plont, S., Shogren, A. J., Tatariw, C., et al. (2025). Investigating Spatial and Temporal Nitrogen Dynamics in a Forested Headwater Stream Over the Course of an Annual Drying Event. Journal of Geophysical Research: Biogeosciences, 130(4), e2024JG008522. https://doi.org/10.1029/2024JG008522

Zimmer, M. A., & McGlynn, B. L. (2017). Bidirectional stream–groundwater flow in response to ephemeral and intermittent streamflow and groundwater seasonality. Hydrological Processes, 31(22), 3871–3880. https://doi.org/10.1002/hyp.11301

Zimmer, M. A., & McGlynn, B. L. (2018). Lateral, Vertical, and Longitudinal Source Area Connectivity Drive Runoff and Carbon Export Across Watershed Scales. Water Resources Research, 54(3), 1576–1598. https://doi.org/10.1002/2017WR021718

Zimmer, M. A., Burgin, A. J., Kaiser, K., & Hosen, J. (2022). The unknown biogeochemical impacts of drying rivers and streams. Nature Communications, 13(1), 7213. https://doi.org/10.1038/s41467-022-34903-4

Zipper, S., Wheeler, C. T., Peterson, D. M., Cook, S. C., Godsey, S. E., & Aho, K. (2025). STICr: An open-source package and workflow for stream temperature, intermittency, and

conductivity (STIC) data. Environmental Modelling & Software, 190, 106484. https://doi.org/10.1016/j.envsoft.2025.106484

Zipper, S. C., Hammond, J. C., Shanafield, M., Zimmer, M., Datry, T., Jones, C. N., et al. (2021). Pervasive changes in stream intermittency across the United States. Environmental Research Letters, 16(8), 084033. https://doi.org/10.1088/1748-9326/ac14ec

Water Resources Research

Supporting Information for

Using Physiography to Understand Stream Network Expansion and Contraction Across Spatiotemporal Scales

Delaney M. Peterson[1,2], C. Nathan Jones[1], Kaci Zarek[1,3], Michelle Wolford[1], Chelsea R. Smith[1], Charles T. Bond[4], Stephen Plont[1], Maggi Kraft[5], Shannon Speir[6], Sam Zipper[7,8], Sarah E. Godsey[5], Jonathan P. Benstead[1], Arial J. Shogren[1], Kevin A. Kuehn[4], and Carla L. Atkinson[1]

[1]Department of Biological Sciences, University of Alabama, Tuscaloosa, AL, USA.

[2]Department of Biological and Ecological Engineering, Oregon State University, Corvallis, OR, USA.

[3]Department of Ecology and Evolutionary Biology, Cornell University, Ithaca, NY, USA.

[4]School of Biological, Environmental, and Earth Sciences, University of Southern Mississippi, Hattiesburg, MS, USA.

[5]Department of Geosciences, Idaho State University, Pocatello, ID, USA.

[6]Department of Crop, Soil, and Environmental Sciences, University of Arkansas, Fayetteville, AR, USA.

[7]Kansas Geological Survey, University of Kansas, Lawrence, KS, USA.

[8]Department of Geology, University of Kansas, Lawrence, KS, USA.

Contents of this file

Introduction

This document contains more detailed site information (Text S1), study design and sensor placement (Figures S1-4), description of all physiographic metrics (Table S1), and proof of calculations following Prancevic & Kirchner (2019; Figure S5) to provide further details on methodology. Additionally, this document contains additional results (Table S2), sensitivity analyses (Table S3, Figures S6-7), random forest statistical outputs (Table S4) as well as additional figures that provide more context to results (Figure S8-9).

Text S1 – Detailed Site Descriptions.

We instrumented three research watersheds across a physiographic gradient in Alabama, USA to evaluate network expansion and contraction across comparably-sized non-perennial streams. In

addition to the details provided in Section 2.1 and Table 1, we have included more detailed watershed characteristics below.

Appalachian Plateaus Research Watershed

The research watershed in the Appalachian Plateau province drains 2.97km^2 of Fanning Hollow and Miller Mountain to form the steep headwaters of Burks Creek, within the larger Paint Rock River and Tennessee River basins. Physiographically, this research watershed is in the Jackson Mountains district, defined by flat sandstone-capped ridges that are highly dissected by dendritic stream networks that form V-shaped ravines and rock-walled gorges as they grade into wider valley bottoms (Swenson, 1945; Sapp & Emplaincourt, 1975).

Geologically, this watershed cuts through and exposes several distinct sedimentary lithologic units. In this region, the plateaus are primarily from the Pottsville and Pennington Formations, which are underlain by the Bangor limestone, Monteagle limestone, and Tuscumbia limestone units, respectively (Szabo et al., 1988; Ponta, 2018). The Pottsville and Pennington formations are primarily sandstones and shales interbedded with limestone, dolomite, and mudstones, whereas the three underlying units are primarily limestone and dolomite with some chert concretions in the Tuscumbia unit (Szabo et al., 1988). Further, the Bangor, Monteagle, and Tuscumbia limestone units are all karst, with the majority of caves in the state occurring in the Bangor limestone unit (Ponta, 2018). The Pottsville formation, Bangor limestone, and Tuscumbia limestone are the primary water-bearing units for the region, with the Pottsville formation being the largest water source in the region and the Bangor limestone being an unconfined karst aquifer that discharges through many springs (Ponta, 2018). This watershed primarily has SSURGO soil map units of Limestone rockland rough and Muskingum Rough stony land. These map units consist of highly organic soils and limestone residuum in the headwaters, and more developed, argillic soils in the valley bottom (Soil Survey Staff, 2025). The dominant soil series are the Barfield, Gorgas, and Egam series.

This watershed is located in the Plateau Escarpment level IV ecoregion, and therefore the forest structure is primarily deciduous, with mixed oak species (chestnut oak, white and red oaks) in the upper slopes, mesic forest (beech, yellow-poplar, sugar maple, basswood, ash, buckeye) in the middle and lower slopes, and some hemlock and river birch in the riparian zones and floodplain terraces near the outlet (Griffith et al., 2001).

Piedmont Research Watershed

The research watershed in the Piedmont province drains 0.92km^2 of Rattlesnake Mountain to form the headwaters of Pendergrass Creek, within the larger Coosa River and Mobile-Tombigbee River basins. Physiographically, this watershed is in the Northern Piedmont Upland district, defined as a well-dissected mature upland in the transition between the nearby Ridge and Valley and Coastal Plain regions (Kopaska-Merkel et al., 2000).

Geologically, this watershed is underlain by fractured metamorphic lithologic units. The watershed is located in the Talladega belt near the Talladega fault, and lies within the exposed Lay Dam formation, which is made up of interbedded phyllite, metasiltstone, and quartzite

members (Szabo et al, 1988; Cook, 1982; Kopaska-Merkel et al., 2000). Productivity of the groundwater system in the Piedmont is driven by fractures rather than geologic material (Kopaska-Merkel et al., 2000), and the proximity of this location to the Talladega fault has likely resulted in a productive groundwater system where the fractures intersect with the soil and ground surface. This watershed has highly weathered soils, with the primary soil series being the Cheaha, Tatum, and Fruithurst, as well as some more organic, fine-grained soils near the watershed outlet (Soil Survey Staff, 2025; Zarek et al., 2025).

The watershed is located within the Talladega Upland level IV ecoregion, and therefore has a mixed deciduous-coniferous forest structure. The region has an oak-hickory-pine natural vegetation type and historically contained unique montane longleaf pine communities (Griffith et al., 2001). The watershed now contains primarily pine and oak species (loblolly, longleaf, mixed red and white oaks; Feminella, 1996; Zarek et al., 2025). While the larger region has a long-term land-use history of intensive cultivation (Trimble, 2008, Griffith et al., 2001), the region transitioned to silviculture around the turn of the 20th century. Additionally, the US Forest Service maintains a regular burn schedule within the National Forest to preserve the longleaf pine and endangered red cockaded woodpecker habitat. As a result, this watershed experienced low-intensity prescribed burns in the early spring of both 2022 and 2024.

Coastal Plain Research Watershed

The research watershed in the Coastal Plain province drains 0.70km^2 of the headwaters of Shambley Creek, within the larger Sipsey River and Mobile-Tombigbee River basins. Physiographically, this watershed is in the Fall Line Hills district, defined by low-gradient sandy uplands that are dissected by severely entrenched streams (Kidd & Lambeth, 1995; Fenneman, 1938).

Geologically, this watershed is underlain by sedimentary lithologic units. The watershed is located in the exposed Eutaw Formation, which consists of interbedded sand and clay layers (Szabo et al., 1988). This formation includes the Tombigbee Sand Member, and the shallow depth to this aquifer results in this unit being an integral water-bearing unit for the region (Wahl, 1966). The primary soils present in this watershed are the Magnolia, Shubuta, Falaya, and Ochlockonee series (Soil Survey Staff, 2025).

Greene County, as well as the larger Coastal Plain of the Southeastern US, has a long-term land-use legacy of intensive agriculture that has resulted in soil degradation and erosion (Trimble, 2008; AL Historical Commission, 2002). The region was heavily used for cotton farming throughout the 19th century before conversion to pine plantations and other silvicultural practices during the southern USA lumber boom circa 1900 (AL Historical Commission, 2002; Fickle, 2014). This property was purchased by the Weyerhaeuser Company and has been used for both rotational pine harvest and forest biofuel research from 2010-2016 (Chescheir et al., 2018; Dobbs, 2016). The watershed is located within the larger Fall Line Hills level IV ecoregion, and therefore has a historic forest structure of mixed coniferous and deciduous species (primarily oaks, hickory, and pines, with some longleaf reintroduction efforts; Griffith et al., 2001).

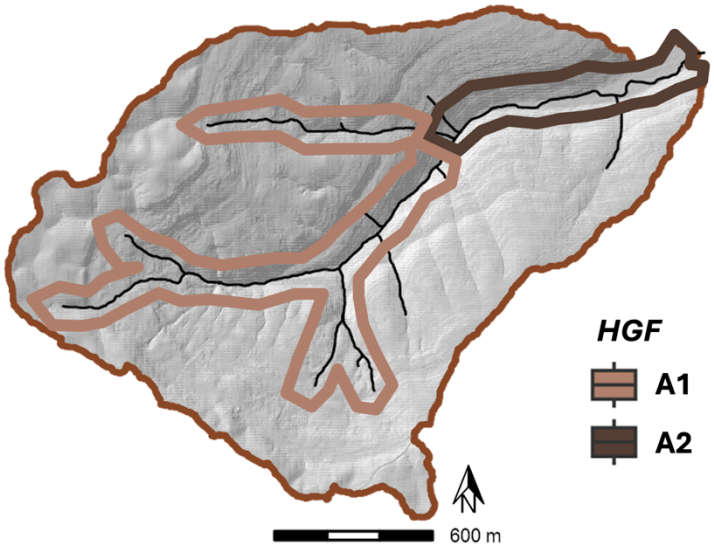

Figure S1. Hydrogeomorphic features of the instrumented portions of the Appalachian Plateaus watershed.

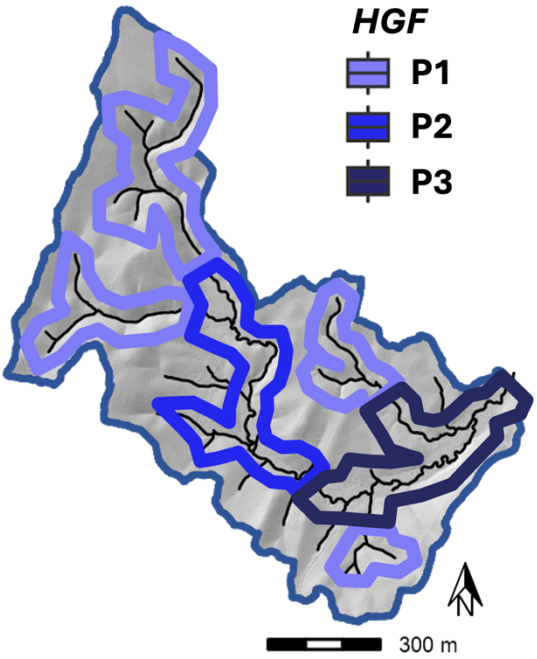

Figure S2. Hydrogeomorphic features of the instrumented portions of the Piedmont watershed.

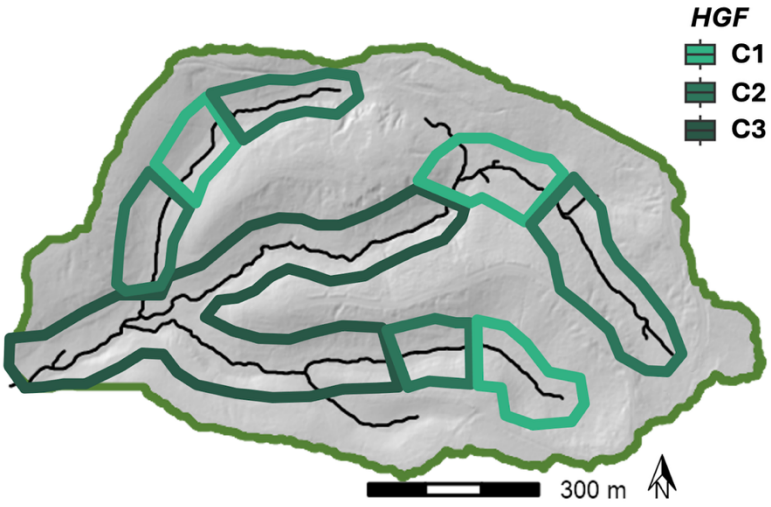

Figure S3. Hydrogeomorphic features of the instrumented portions of the Coastal Plain watershed.

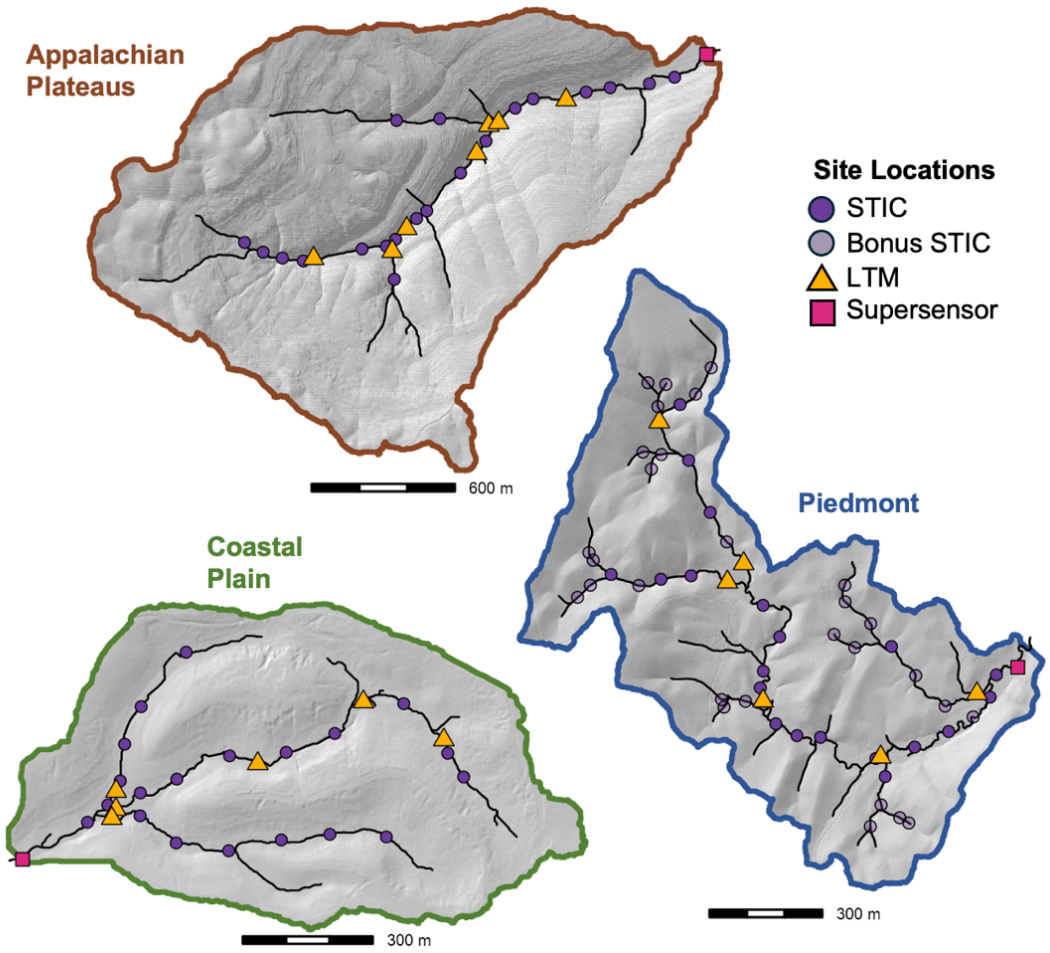

Figure S4. Sensor networks of the three research watersheds. Each watershed shows the three different types of sensors present (STIC = water presence/absence; Bonus STIC = the high-density additional sensors deployed in the Piedmont research watershed; LTM = Long-Term Monitoring locations, where stilling wells and piezometers were deployed in the channel and regular water sampling occurred; Supersensor = the outlet monitoring location, where water level and discharge were measured, as well as a high-frequency water quality sonde).

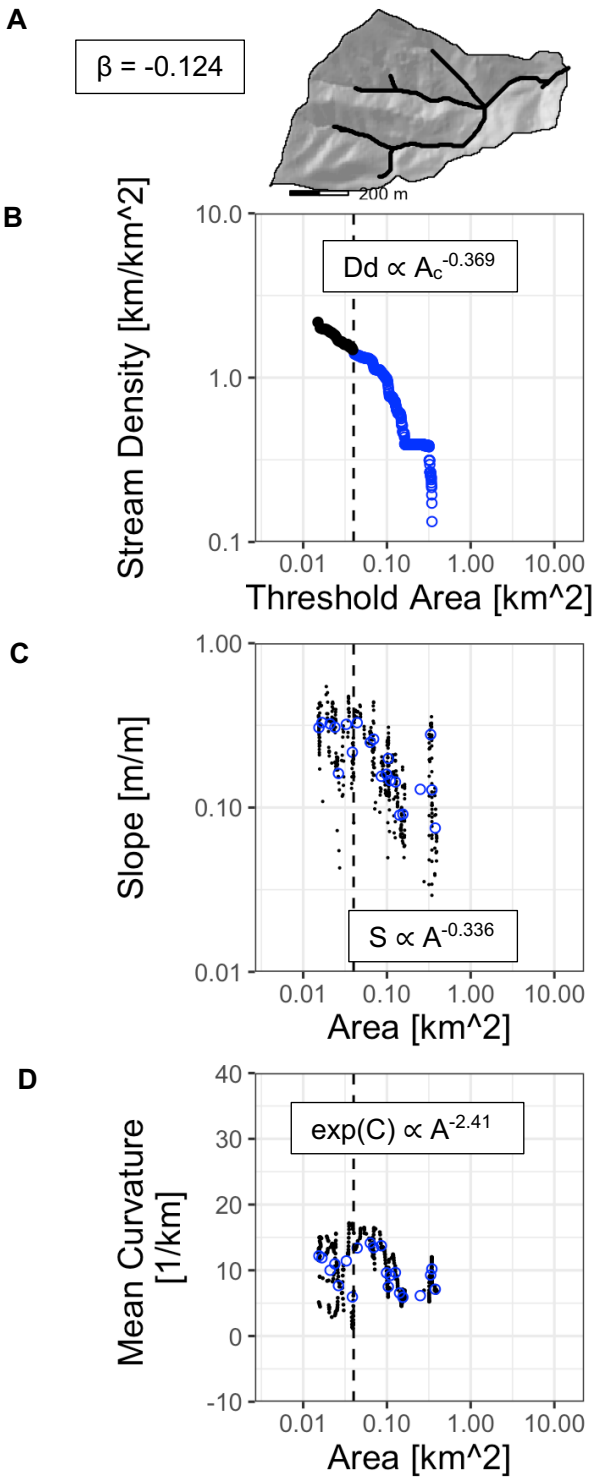

Figure S5. Validation of topographic analyses using Coweeta 40 from Prancevic & Kirchner (2019). (A) Manually delineated watershed. (B) Network observations of stream density, where the ephemeral network used to calculate α indicated by black points. (C) Network slope, where binned averages used to calculate θ indicated by blue points. (D) Network curvature, where binned averages used to calculate δ indicated by blue points.

Table S1. A description of all physiographic metrics calculated for this study.

Category	Metric	Scale	Description	Reference
Topographic	Slope	Site (1m)	Slope (%) extracted from the DEM at the sensor location using *wbt_slope()*	Lindsay, 2016; Florinsky, 2016
	Buffer slope	Site (5m)	Slope (%) averaged in a 5m circular buffer around the sensor location using *wbt_slope()*	sensu Warix et al., 2023; Lindsay, 2016
	Channel Slope	Reach (25m)	Slope (%) of only the channel network averaged across a 25m reach using *wbt_stream_slope_continuous()*	Lindsay, 2016
	Curvature	Site (1m)	Mean curvature (m^{-1}) of the topographic surface using *wbt_mean_curvature()*, doubled with the sign reversed to following Prancevic & Kirchner (2019)	Wilson, 2018; Lindsay, 2016; Prancevic & Kirchner (2019)
	Distance to outlet	Site	In-stream distance (m) from watershed outlet to sensor location using *wbt_distance_to_outlet()*	Lindsay, 2016
	Drainage area	Site	Contributing area (m^2) draining to an individual sensor location using *wbt_d8_flow_accumulation()*	Lindsay, 2016
	Topographic Wetness Index (TWI)	Site (1m)	TWI of the sensor location calculated as **ln(catchment area / tan(slope))** using *wbt_wetness_index()*	Beven & Kirkby, 1979; Lindsay, 2016
	Topographic Position Index (TPI)	Site (5m)	TPI of the 5m circular buffer around the sensor calculated as (focal elevation - mean(all other cell elevations)) using *TPI()*	Ilich et al., 2025
	Drainage density	Site	Upstream length (m) divided by drainage area of the sensor location	Montgomery & Dietrich, 1989; Godsey & Kirchner, 2014
	α, drainage density exponent	Network	The scaling exponent of the relationship between drainage area and distance downstream, calculated as length as a function of activation area threshold ($L \propto A_h^{-\alpha}$)	Prancevic & Kirchner, 2019
	θ, slope exponent	Network	The scaling exponent of the relationship between slope and drainage area, calculated as length as a function of drainage area ($S \propto A^{-\theta}$)	Prancevic & Kirchner, 2019
	δ, curvature coefficient	Network	The coefficient of the relationship between topographic curvature and drainage area, calculated as ($C = \delta \ln A + C_0$)	Prancevic & Kirchner, 2019
	β, network expansion exponent	Network	The exponent of the relationship between stream length and discharge at the outlet, calculated as ($L \propto Q_o^{\beta}$)	Godsey & Kirchner, 2014; Prancevic & Kirchner, 2019
	γ, transmissivity exponent	Network	The scaling exponent of the theoretical relationship between transmissivity and	Prancevic & Kirchner, 2019

			drainage area, calculated as transmissivity as a function of drainage area ($T \propto A^{-\gamma}$)	
Soil	Saturated hydraulic conductivity	HGF	Ability of saturated pores to transmit water (µm/s) in the upper 100 cm of the soil profile for each soil map unit, derived from soil structure, porosity, and texture data	Soil Survey Staff, 2025
	Percent sand	HGF	Sand textural content (%) in the total soil profile as a weighted average for each soil map unit	Soil Survey Staff, 2025
	Percent silt	HGF	Silt textural content (%) in the total soil profile as a weighted average for each soil map unit	Soil Survey Staff, 2025
	Percent clay	HGF	Clay textural content (%) in the total soil profile as a weighted average for each soil map unit	Soil Survey Staff, 2025
	Organic matter content	HGF	Organic matter (%) by weight in the upper 50 cm of the soil profile for each soil map unit	Soil Survey Staff, 2025
Geology	Primary lithologic unit	HGF	Most surficial geologic layer; identified as parent material from soil surveys for each soil map unit	Soil Survey Staff, 2025; Szabo et al., 1988
	Depth to bedrock	HGF	Average depth (cm) to a lithologic restrictive layer for each soil map unit	Soil Survey Staff, 2025
Vegetation	Percent coniferous vegetation	HGF	Relative percentage of coniferous vegetation (%), derived from the difference between leaf off and leaf on densiometer measurements	

Table S2. All topographic coefficients calculated for the study.

Watershed	**Predicted** expansion exponent, β	**Observed** expansion exponent, β	Drainage density exponent, α	Slope exponent, θ	Transmissivity exponent, γ	Curvature coefficient, δ
Appalachian Plateaus (Burks Creek)	0.042	0.185 ±0.086	0.387	0.525	0.567	5.49
Piedmont (Pendergrass Creek)	0.170	0.076 ±0.039	0.413	0.390	4.04	1.03
Coastal Plain (Shambley Creek)	0.840	0.127 ±0.087	0.417	0.289	1.99	-0.188
Providence Creek[a]	0.34	0.401 ±0.061	0.576	0.02	0.42	0.74
Bull Creek[a]	0.14	0.182 ±0.022	0.399	0.165	1.03	1.37
Caspar Creek[a]	0.277	0.31 ±0.050	0.469	0.726	-0.21	0.3
Sagehen Creek[a]	0.3	0.312 ±0.093	0.419	0.284	0.06	0.39
McDonald 1[b]	0.095	0.058 ±0.015	0.484	0.487	2.95	2.59
McDonald 2[b]	0.062	0.109 ±0.040	0.675	0.081	10.56	6.49
Elder Creek[c]	0.219	0.175 ±0.037	0.487	0.402	1.38	0.83
Cougar Creek[d]	0.098	0.083 ±0.100	0.379	0.238	3.33	1.96
Dunce Creek[d]	0.086	0.093 ±0.013	0.442	0.126	3.63	2.81
Goat Creek[d]	0.112	0.055 ±0.024	0.245	0.257	3.19	0.9
Pioneer Creek[d]	0.24	0.197 ±0.037	0.595	0.339	1.68	1.03
Yellow Barn[e]	0.168	0.114 ±0.040	0.49	0.273	3.02	1.35
Coweeta 40[f]	-0.14	0.040 ±0.008	0.384	0.39	8.21	-2.32

Fernow 37[f]	0.195	0.180 ±0.017	0.593	0.173	2.12	1.49
Hubbard 25[f]	0.15	0.590 ±0.033	0.28	0.076	-0.6	0.81
Hubbard 42[f]	0.166	0.240 ±0.023	0.578	0.128	1.28	1.79
S. Fork Potts 70[f]	0.089	0.140 ±0.006	0.542	0.393	2.48	3.26

Note: All variables retrieved from Prancevic & Kirchner (2019)
[a]Originally from Godsey & Kirchner (2014)
[b]Originally from Roberts & Klingeman (1972)
[c]Originally from Lovill et al. (2018)
[d]Originally from Whiting & Godsey (2016)
[e]Originally from Shaw (2016)
[f]Originally from Jensen et al. (2017)

Table S3. Sensitivity analysis for the relationship between temporal resolution and expansion exponent, β.

Watershed	15-minute β	Mean Daily β	Daily Noon β
Coastal Plain	0.085 ± 0.076	0.121 ± 0.098	**0.127** ± 0.087
Appalachian Plateaus	0.204 ± 0.085	0.161 ± 0.092	**0.185** ± 0.086
Piedmont (n = 20)	0.059 ± 0.033	0.082 ± 0.039	**0.076** ± 0.039
Piedmont (n = 49)	0.058 ± 0.048	0.061 ± 0.047	**0.059** ± 0.048

Note: β in bold were used in analyses.

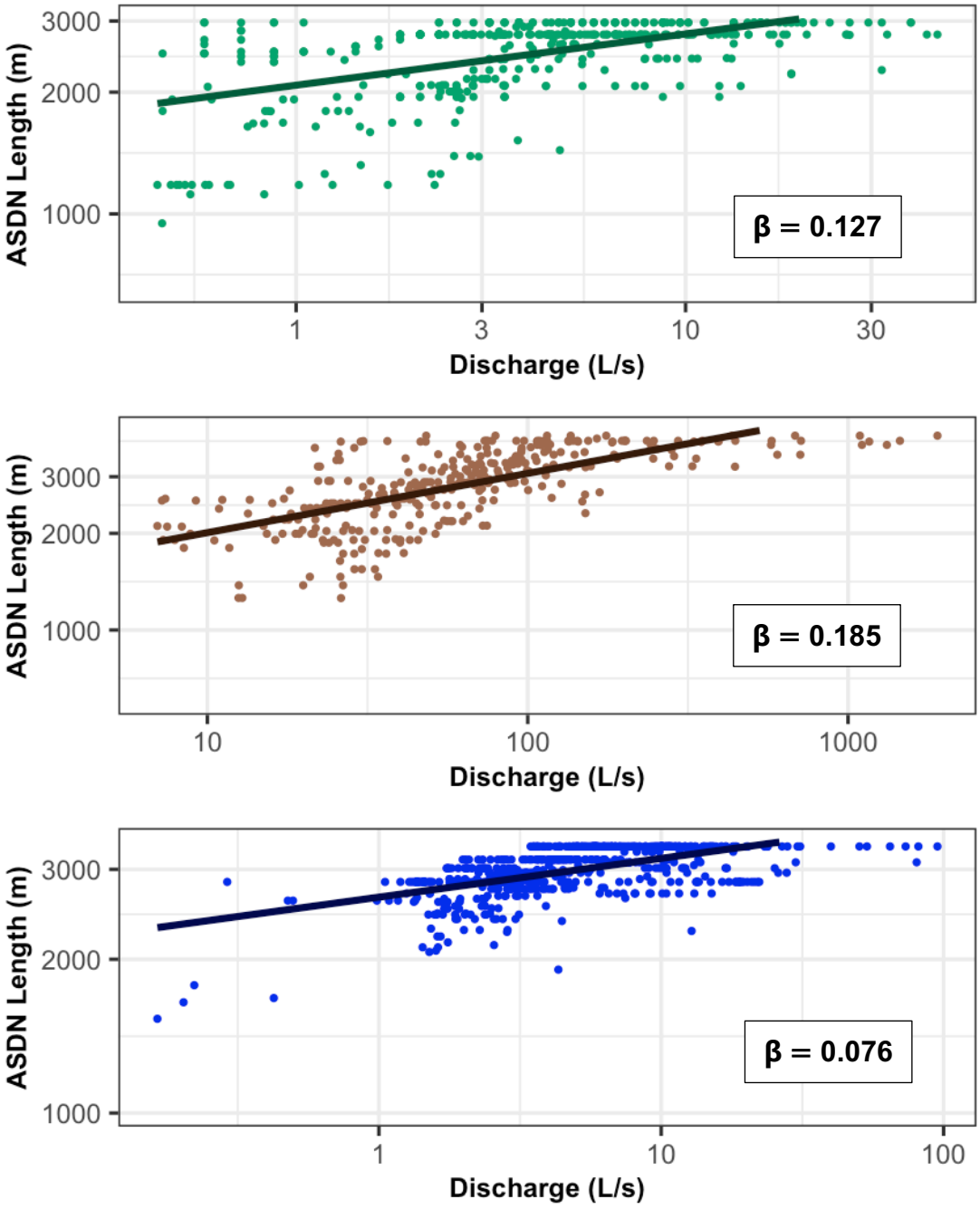

Figure S6. Daily observations of outlet discharge (Q) and network length used to calculate observed expansion exponents (β) for each watershed. Coastal Plain is indicated in green, Appalachian Plateaus in brown, and Piedmont in blue.

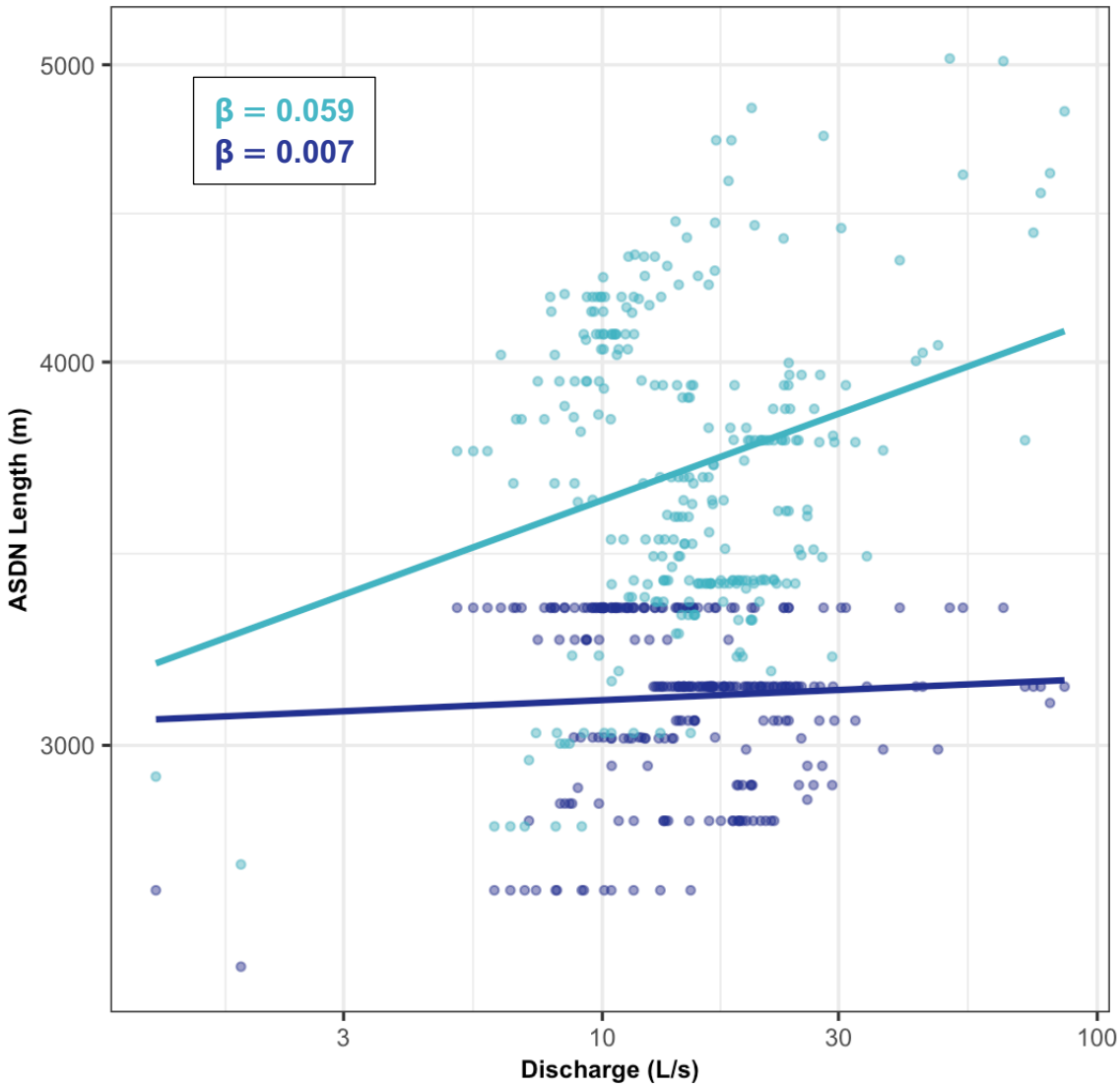

Figure S7. Daily observations of outlet discharge (Q) and network length used to calculate observed expansion exponents (β) for both the high density (n = 49; light blue) and permanent (n = 20; dark blue) sensor networks in the Piedmont watershed. Note: data from the 11-month period of high-density deployment is used here to ensure comparability, rather than the two water years used in other analyses.

Table S4. Random Forest model results

Data	Model	R^2	RMSE	MAE	MAPE
Test	Coastal Plain	0.56	0.07	0.05	9.6
	Piedmont	0.75	0.15	0.12	18.5
	Appalachian Plateaus	0.16	0.24	0.21	42.6
	Global	*0.10*	*0.23*	*0.18*	*42.7*
Train	Coastal Plain	0.92	0.09	0.07	30.8
	Piedmont	0.92	0.08	0.06	11.9
	Appalachian Plateaus	0.88	0.10	0.08	23.5
	Global	*0.95*	*0.09*	*0.07*	*23.7*

Note: models were evaluated using Root Mean Squared Error (RMSE), coefficient of determination (R^2), Mean Absolute Error (MAE), and Mean Absolute Percent Error (MAPE)

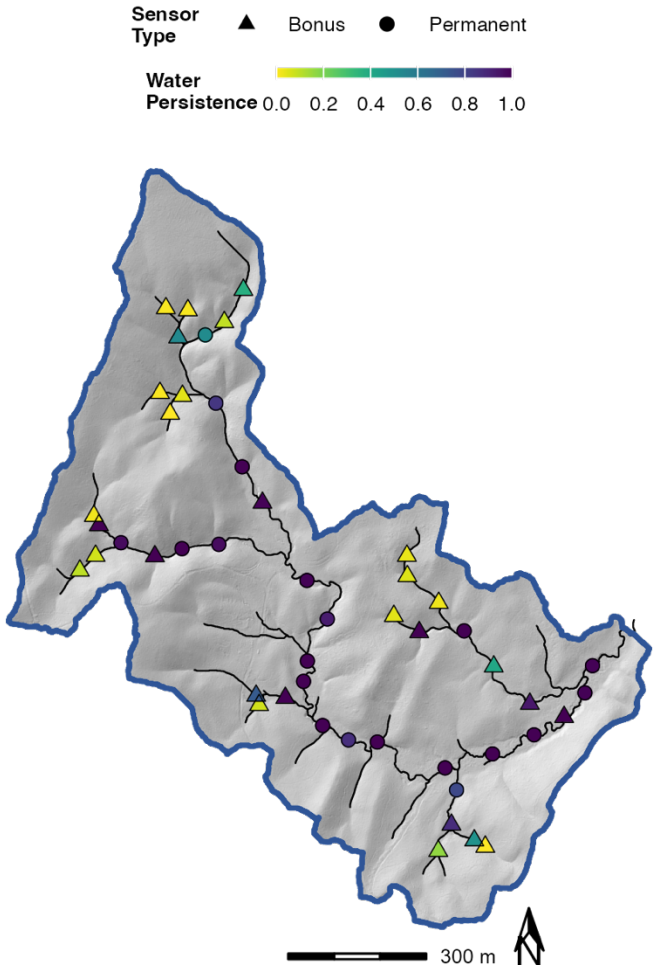

Figure S8. The Piedmont research watershed, with each site colored by water persistence over the 11-month period of high-density sensor deployment. Permanent sensors (n = 20) are indicated by circles, and the additional high-density network sensors (n = 29) are indicated by triangles. Water persistence is measured as the proportion of days the sensor recorded "wet" from May 2022 through April 2023.

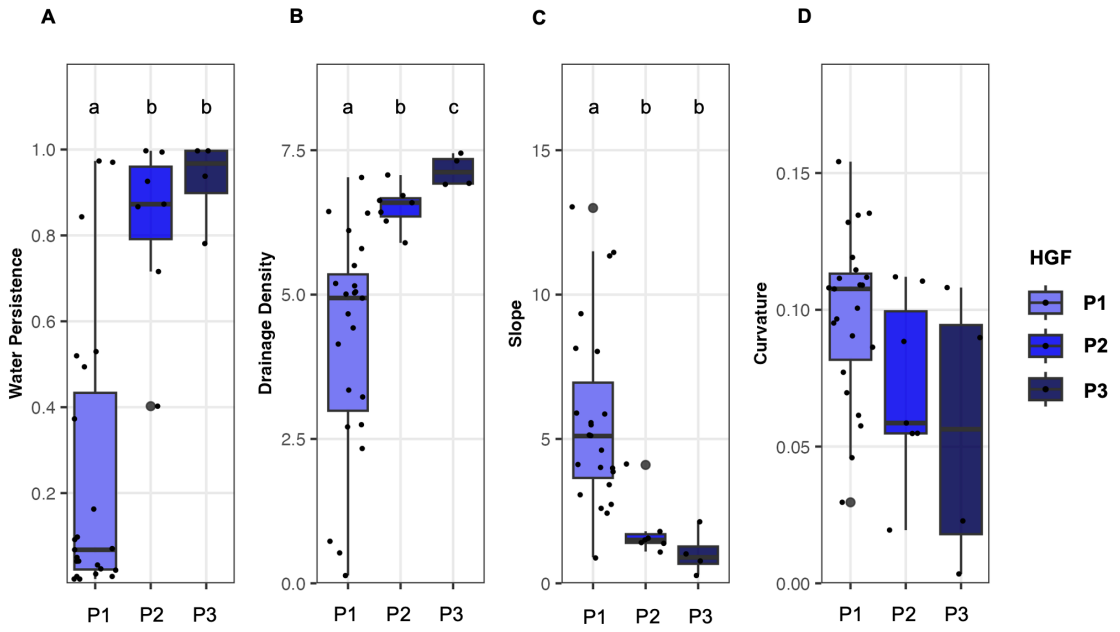

Figure S9. Boxplots for water persistence (A) and the three primary topographic metrics (B-D) for all sensors in the Piedmont high-density network (n = 49). Sensors are grouped by hydrogeomorphic feature (HGF, see legend and x axis). Significance between groups is denoted by letters above each group (p < 0.05). See Figure 8 for continuous relationships between water persistence (A) and subsequent topographic metrics (B-D).